Changes of the tropical glaciers throughout Peru between 2000 and 2016 – Mass balance and area fluctuations

Seehaus Thorsten[1], Malz Philipp[1], Sommer Christian[1], Stefan Lippl[1], Alejo Cochachin[2],Matthias Braun[1]

[1]Institute of Geography, Friedrich-Alexander-University Erlangen-Nuremberg, Wetterkreuz 15, 91058 Erlangen, Germany

5   [2]Unidad de Glaciología y Recursos Hídricos (UGRH), Autoridad Nacional del Agua (ANA), 02001 Huaraz, Perú

Correspondence to: Thorsten Seehaus (thorsten.seehaus@fau.de)

Abstract. Glaciers in tropical regions are very sensitive to climatic variations and thus strongly affected by climate change. The majority of the tropical glaciers worldwide are located in the Peruvian Andes, which have shown significant ice loss in the last century. Here, we present the first multi-temporal, region wide survey of geodetic mass balances and glacier area

10   fluctuations throughout Peru covering the period 2000-2016. Glacier extents are derived from Landsat imagery by performing automatic glacier delineation based on a combination of the NDSI and band ratio method and final manual inspection and correction. The mapping of debris-covered glacier extents is supported by SAR-coherence information. A total glacier area loss of -548.5±65.7 km² (-29%, -34.3 km² a⁻¹) is obtained for the study period. Using interferometric satellite SAR acquisitions, bi-temporal geodetic mass balances are derived. An average specific mass balance of -296 ± 41 kg m^{-2} a^{-1} is found throughout

15   Peru for the period 2000-2016. However, there are strong regional and temporal differences in the mass budgets ranging from 45 ± 97 kg m^{-2} a^{-1} to -752 ± 452 kg m^{-2} a^{-1}. The ice loss increased towards the end of the observation period. Between 2013 and 2016, a retreat of the glacierised area of -203.8±65.7 km² (-16%, -101.9 km² a⁻¹) is mapped and the average mass budget amounts to -660 ± 178 kg m^{-2} a^{-1}. The glacier changes revealed can be attributed to changes in the climatic settings in the study region, derived from ERA-Interim reanalysis data and the Oceanic Niño Index. The intense El Niño activities in 2015/16 are

20   most likely the trigger for the increased change rates in the time interval 2013-2016. Our observations provide fundamental information on the current dramatic glacier changes for local authorities and for the calibration and validation of glacier change projections.

1   Introduction

Tropical glaciers in the Peruvian Andes are very sensitive to climate change and rapidly respond to varying climate settings (e.g. Kaser and Osmaston, 2002; Rabatel et al., 2013). A marked decrease in glacier coverage in Peru has be reported by various

25   studies (e.g. Georges, 2004; Hanshaw and Bookhagen, 2014; Vuille et al., 2008) for the last decades. The recession of the Peruvian glaciers is proposed to have significant impact on the downstream ecosystem and communities (Vuille et al., 2018). Glaciers act as an important temporal water reservoir for precipitation during the wet season. Glacier meltwater runoff buffers the water shortage caused by the low precipitation during the dry season (Kaser et al., 2003; Schauwecker et al., 2017). The shrinkage of glaciers leads to higher meltwater discharge and thus increases water supply to streamflow. However, glacier

30   runoff decreases after the glacier loss reaches a critical transition point (Pouyaud et al., 2005). It has been suggested that some watersheds in the Cordillera Blanca have already crossed this critical transition point (Baraer et al., 2012). An unsteady or unreliable water runoff is known to cause several socio-economic issues (Drenkhan et al. 2019). Hydropower production and mining rely on a continuous water supply. Moreover, glacier runoff is an important water resource for irrigation and has the

potential to affect large-scale but also subsistence agriculture (Vuille et al., 2018). It also impacts the Andean ecosystems. For example, the *bofedales* (high-altitude wet lands in the Andes) are very sensitive to changes in glacier runoff and a depletion of the meltwater is likely to cause them to shrink (Polk et al., 2017). Additionally, the glacier retreat leads to the formation and extension of pro-glacial lakes (Hanshaw and Bookhagen, 2014; Lopez et al., 2010) threatening downstream areas due to their potential to cause glacier lake outburst floods (GLOF). In the Cordillera Blanca, several GLOFs have harmed local communities in the past. The most dramatic was the disaster in 1941 when large parts of the city of Huaraz were destroyed by a GLOF event, leading to ~1800 casualties (Carey, 2010). However, GLOF threats are present throughout the Tropical Andes (Cook et al., 2016; Hoffmann, 2012).

Several studies have been carried out to map and quantify changes in the glacier area in Peru. The majority of the analyses have focused on Peru's largest glacierised region, the Cordillera Blanca (e.g. Baraer et al., 2012; Georges, 2004; Hastenrath and Ames, 1995; Racoviteanu et al., 2008; Silverio and Jaquet, 2005, 2017; Unidad de Glaciologia y Recursos Hidricos (UGRH), 2010), and revealed significant glacier retreat in the last decades. The most recent studies reported a glacier recession in the Cordillera Blanca of -46% between 1930 and 2016 (Silverio and Jaquet, 2017) and -33.5% between 1975 and 2016 (Veettil, 2018). In other glacierised regions in Peru, distinct glacier retreat was observed as well. In the second largest glacierised mountain range in Peru, the Cordillera Vilcanota, an area loss of -32% in the period 1985-2006 (Salzmann et al., 2013) and -30% in the period 1988-2010 (Hanshaw and Bookhagen, 2014) was revealed. The only countrywide estimation of glacier area changes was carried out by the UGRH (2014). They estimated a total glacier retreat of -42.64% from the first Peruvian glacier inventory of 1970 (Hidrandina SA, 1989) and the recent inventory covering the period 2003-2010 (UGRH, 2014). So far, no multi-temporal nor recent quantification of glacier area changes throughout Peru is available, only studies at regional levels.

There are a few studies dealing with surface elevation and ice volume/mass changes in Peru. Changes in the ice volume of -57*10^{-6} m³ have been derived from aerial photographs and GPS point measurement data for three glaciers in the Cordillera Blanca by Mark and Seltzer (2005) for the period 1962-1999. Huh et al. (2017) calculated the surface elevation changes of six glaciers in the Cordillera Blanca by means of photogrammetric digital elevation models (DEMs) and LiDAR measurements. They found glacier wide average surface lowering ranging between -9.5 and -64.06 m in the period 1962-2008. In the Cordillera Vilcanota, Salzmann et al. (2013) estimated volume changes of -40 to -45% based on inventory parameters for the period 1962-2006. Large-scale mass balance estimates covering Peru are the following: a mass balance estimation for the "low latitudes" of -1080±360 kg m^{-2} a^{-1} based on the upscaling of glaciological mass balance measurements covering the period 2003-2009 (Gardner et al., 2013); modelled surface mass balance of -1550±620 kg m^{-2} a^{-1} for the Andes north of 27°S in the period 1979-2014 (Mernild et al. 2017), a upscaled mass balance of -2 ± 2 Gt a^{-1} (-1030 ± 830 kg m² a^{-1}) for the same region using glaciological and geodetic mass balances between 2006 and 2016 (Zemp et al. 2019), a mass balance calculation throughout South America (excluding Patagonia) of -6±12 Gt a^{-1} using space borne gravimetric measurements from the Gravity Recovery and Climate Experiment (GRACE) for the period 2000-2010 (Jacob et al., 2012); and a geodetic mass budget of -0.49±0.09 Gt a^{-1} (-227±42 kg m^{-2} a^{-1}, ice density scenario: 850 kg m^{-3}) derived from InSAR measurements for the period 2000-2012/13 including glaciers in Bolivia (Braun et al., 2019). The first three cover large areas and thus the mass balance signals of glaciers in Peru or even smaller regions cannot be derived. The latter uses the glacier boundaries defined by the Randolph Glacier Inventory (RGI) 6.0. The RGI 6.0 has certain limitations in this region (RGI Consortium, 2017), which can lead to biases in the mass balance computation (Section 6.2).

Up to now, a spatially detailed and multi-temporal quantification of glacier changes throughout Peru is missing. In order to address this issue, this work aims to continue and expand the glacier monitoring of previous studies by carrying out a

2

comprehensive analysis of glacier area changes and mass balances throughout the Peruvian Cordilleras for the observation period 2000-2016 based on multi-sensor remote sensing data. The main objectives of this study are:

- to obtain a temporally and methodically consistent evaluation of countrywide glacier area changes

- to assess geodetic glacier mass balances and their temporal variations throughout Peru

- to identify relations between glacier fluctuations, changes of climatic variables and topographic parameters

2 Study site

Peru is home to the majority of tropical glaciers worldwide. About 70% of all tropical glaciers, covering an area of 1602.96 km² (RGI 6.0), are located there. The Peruvian Andes are subdivided into three major mountain ranges, the Cordillera Occidental, Central and Oriental, from west to east, and several smaller Cordilleras (Figure 1). According to Sagredo and Lowell (2012), the glacierised areas are divided into three subregions based on their climatic settings:

- R1: Northern wet outer tropics, with a high mean annual humidity of 71%, nearly no seasonality of the temperature (annual mean: 1.6 °C; variability of mean monthly temperature ~1 °C) and a total annual precipitation of 815 mm. R1 ranges from the Cordillera Blanca southwards to the Cordillera Chonta and also includes the Cordilleras Huagoruncho and Huaytapallana further east.

- R2: Southern wet outer tropics, with moderate mean annual humidity of 59%, an annual variability of the mean monthly temperature of about 4 °C (annual mean: 1.6 °C) and a total annual precipitation of 723 mm. R2 ranges from the Cordillera Vilabamba westwards to the Cordillera Apolobamba (partly located in Bolivia, but included completely in this study).

- R3: Dry outer tropics, with low mean annual humidity of 50%, a mean annual temperature of -4.0 °C (variability of the mean monthly temperature of ~5°C) and low total annual precipitation of 287 mm. R3 ranges from the Cordillera Ampato westward to the Cordillera Volcanica.

The annual variability of precipitation shows a strong seasonality in all three subregions (Sagredo and Lowell, 2012) with a dry season during austral winter from May to September and a wet season during austral summer from October to April. The glaciers accumulate mass almost exclusively during the wet season, whereas the lower reaches of the glaciers experience ablation throughout the year (Kaser, 2001). Thus, slight variations in precipitation and temperature can lead to strong changes of the glacier mass balances (Francou Bernard et al., 2003), but also surface albedo and radiation significantly affect the mass budget of tropical glaciers (Favier et al., 2004; Wagnon et al., 1999). Moreover, the reaction of the glaciers in the Tropical Andes to changing environmental conditions is nearly immediate (Vuille et al., 2008). The El Niño Southern Oscillation (ENSO) has a strong impact on climate and thus the glacier mass balances in Peru (Garreaud et al., 2009; Maussion et al., 2015). El Niño events typically lead to pronounced glacier mass losses due to an induced precipitation deficit and above

3

average temperatures, whereas during La Niña periods the opposite conditions lead to reduced mass losses or even mass gain (Favier et al., 2004; Vuille et al., 2008).

105 Glaciological mass balance measurements are carried out at several glaciers in the study region by the UGRH, a subdivision of the Autoridad Nacional del Aqua (National Water Administration). However, observations are available in the World Glacier Monitoring Service (WGMS) database only for two glaciers covering our study period 2000-2016. Continuous annual mass balance observations have been documented at Artesonraju Glacier and Yanamarey Glacier since 2004. At some additional glaciers, mass balance programmes were initiated later and the data are not yet archived in the WGMS database.

3   Data

110 Spaceborne remote sensing data from different sensor systems are collected to perform this comprehensive study on glacier changes in the period 2000-2016. Synthetic Aperture Radar (SAR) data are used to obtain information on glacier surface elevation changes and mass balances. Digital elevation models (DEM) derived from interferometric SAR acquisitions at different time steps are used to compute surface elevation change information. As the elevation reference at the start of our observation interval, the void-fill LP DAAC NASA Version 3 SRTM DEM (NASA JPL, 2013) is used. It is based on bistatic

115 C-band SAR data, acquired during the Shuttle Radar Topography Mission (SRTM) by the National Aeronautics and Space Administration (NASA) and the German Aerospace Center (DLR) in February 2000. DEMs of later dates are generated from bistatic X-band SAR imagery of DLR's TanDEM-X (TDX) mission, which started in 2010 (Zink et al., 2011) (Section 4.2). Both SAR missions acquired data using different radar bands. Signal penetration of different radar frequencies in glacier surfaces depends on water content and the density of upper layers. This can lead to biases when comparing elevations on

120 glacierised areas. Thus, we tried to select only imagery from the same season as the SRTM data in order to obtain acquisitions with similar glacier surface conditions and to avoid seasonal mass balance biases. In early 2013, an almost complete coverage of the glacierised regions in Peru could be obtained (early 2012 at subregion R1 as well as for comparison with Braun et al., 2019). Only a small fraction of the glacierised areas in subregion R3 had no coverage by TDX in early 2013. TDX imagery from early 2014 is used to fill the gaps (Section 5.2). A second temporally consistent coverage of the Peruvian glaciers by TDX

125 data is available for 2016, though acquired primarily in the months of October and November, which mark the end of the dry season and beginning of the wet season. Typically negligible accumulation occurs during the dry season and ablation is dominating the glacier mass budget (Favier et al., 2004; Kaser, 2001; Veettil et al., 2017b). Thus, the mass balances for observation periods ending in 2016 are slightly biased towards more negative values due to this seasonal offset in the data. It is difficult to adequately quantify this temporal bias. Therefore, no correction is employed in the analysis and our computed

130 mass loss rates represent upper bound estimations for the periods 2000-2016 and 2013-2016. A summary of the 331 analysed TDX scenes is provided in Table S1 and the spatial coverage of the subregions is plotted in Figure S1.

The RGI 6.0 Region 16 "Low Latitudes" covers all glacierised regions in Peru. The outline dates range between 2000 and 2009 in Peru. Thus, it does not represent the glacier extent at a specific moment. Moreover, it is mentioned in the RGI 6.0

Technical Report (RGI Consortium, 2017) that significant snow contamination caused difficulties in the glacier delineations, especially in southern Peru, and that a more rigorous demarcation could decrease the total glacier area. The Peruvian glacier inventory compiled by UGRH (2014) is also not temporally consistent. It covers the period 2003-2010. In order to use temporally appropriate glacier outlines for the mass balance evaluations and to map coincidental glacier area changes, we decided to generate a consistent database of countrywide glacier extents that correlates with the dates of our coverages of interferometric SAR data (see above). Cloud-free multispectral images from Landsat 5 TM and Landsat 8 OLI are ordered from the United States Geological Survey (USGS). Imagery, preferably during the dry season, is selected to reduce distortions due to temporal snow cover. For all subregions, a complete coverage in 2000 and 2016 is available. In subregions R1 and R2, cloud and snow cover forced us to map a small fraction of the glacierised regions using imagery from 2014 (Section 5.1). An overview of the analysed Landsat imagery is presented in Table S2. The Cordillera Blanca is the only mountain range with a considerable debris-covered glacier fraction. Therefore, the mapping of the glacier extents in this area is supported by interferometric analysis of repeat pass SAR acquisitions from the TerraSAR-X and Sentinel-1 satellite missions.

ERA-Interim reanalysis data (Dee et al., 2011) covering the period 1979-2017 provided by the Center for Medium-Range Weather Forecasts (ECMWF) are used to evaluate climatic changes and to identify correlations between glacier fluctuations, skin temperature, total precipitation and downward surface thermal radiation. Monthly Oceanic Niño Index (ONI) data are applied as a proxy for ENSO events, which is available from the National Oceanic and Atmospheric Administration (NOAA) Climate Prediction Center (http://origin.cpc.ncep.noaa.gov/products/analysis_monitoring/ensostuff/ONI_v5.php). According to NOAA's definition, ONI values above +0.5 indicate El Niño events, whereas La Niña is present when ONI values are below -0.5.

4 Methods

4.1 Glacier inventory

Since the manual delineation of glacier extents is laborious, time-consuming and subjective, several methods have been developed to automatically map glacier outlines based on multispectral images (Veettil and Kamp, 2017). The most widely used and robust approaches are the computation of the normalized difference snow index (NDSI) or the band ratio (BR) and the application of a threshold value to differentiate between on- and off-glacier areas (GLIMS algorithm working group, n.d.; Paul et al., 2013). In this study, we first used the NDSI to classify glacier areas and combined it with BR information to improve the mapping in areas affected by shadows. NDSI maps generated from top of atmosphere reflectance values show a better performance than NDSI maps based on digital number values. For the BR computation, digital number values are taken. The threshold value selection is supported by high-resolution satellite imagery (Google Earth) from the respective dates. A NDSI threshold value of 0.8 is selected, which is higher than the thresholds of 0.5-0.6 applied by other studies in this region (e.g. Silverio and Jaquet, 2005; Veettil et al., 2017). This offset might be induced by the application of top of atmosphere reflectance

5

values instead of digital number values. The threshold for the BR data is set to 1.7 for Landsat 5 TM and 1.5 for Landsat 8 OLI data. Finally, polygons of the glacier outlines are generated from the computed glacier masks.

165 The detection of the debris-covered glacier termini extents in the Cordillera Blanca is difficult using multi-spectral imagery. Therefore, we generated SAR coherence maps from repeat-pass SAR acquisitions to distinguish the debris-covered ice from the surrounding ice-free areas (Atwood et al., 2010; Lippl et al., 2018). The surface structure of the debris-covered glacier areas changes over time due to the dynamics and melting of the underlying ice. This leads to a temporal decorrelation of the backscattered SAR signal of repeat-pass SAR imagery and thus to lower coherence as compared to the surrounding ice-free

170 areas. This difference in coherence facilitates the delineation of the debris-covered ice areas. Data from the Sentinel-1 mission are used to map the debris-covered areas in 2016. No suitable repeat-pass SAR acquisitions are available for the Cordillera Blanca in 2013. Thus, we had to rely on TerraSAR-X and Sentinel-1 data from 2014 to map the outlines of the debris-covered glacier tongues. In 2000 (and ±1 year), only repeat-pass SAR data are available from the European Remote Sensing (ERS) satellite with a repetition cycle of one day. Due to this short temporal baseline, a separation between debris-covered ice and

175 surrounding ice-free areas is unfeasible. Consequently, we combined our outlines from 2000 with the manually delineated debris-cover masks available from the Global Land Ice Measurements from Space (GLIMS) database from 2003 based on SPOT imagery (Racoviteanu, 2005).

The catchment discriminations of the RGI are applied to split the resulting polygons into individual glacier basins. In the next step, the glacier inventories are visually inspected and misclassified areas are manually corrected. These manual corrections

180 are supported by high-resolution imagery from the respective years (Google Earth). According to the RGI 6.0 Technical Report (RGI Consortium, 2017), topographic parameters (minimum, maximum and median elevation, mean slope and aspect) of the individual glacier basins are computed using the void-filled SRTM DEM as an elevation reference. Finally, the areas (S) of the complete inventories and of each glacier are measured in UTM projection (UTM Zone 18S for subregion R1 and UTM Zone 19S for subregion R2 and R3). The uncertainties of the area gauging (δ_S) are calculated following the approach of Malz

185 et al. (2018) based on an error evaluation of 3% for alpine glacier outlines derived from Landsat images (Paul et al., 2013). This estimate is scaled by the area to perimeter ratio of the studied subregion compared to the area to perimeter ratio of Paul et al. (2013) in order to account for differences in the shape of the glacierised areas.

4.2   Elevation change

Surface elevation change information is computed by differencing DEMs from SRTM and TDX data. DEMs are derived from the bistatic TDX imagery following the differential interferometric approach (e.g. Malz et al., 2018; Seehaus et al., 2015; Vijay

190 and Braun, 2016), which is briefly summarized in the following.

First, acquisitions from the same relative orbit and date are concatenated in the along track direction. A differential interferogram is computed using the void-filled SRTM DEM as elevation reference. In the next steps, the interferogram is filtered, unwrapped by applying the branch cut and minimum cost flow algorithm and the unwrapped differential phase is transferred into differential elevations. Subsequently, the topographic information of the SRTM DEM is added to obtain

6

absolute height information and finally the product is geocoded and orthorectified. The DEMs are visually checked for phase-jumps and the best results of both phase-unwrapping methods are selected for further processing. Areas affected by remaining phase-jumps are masked out.

The TDX DEMs need to be precisely horizontally and vertically coregistered to the respective reference DEM (SRTM for 2000, TDX for 2013) in order to accurately map elevation changes on the glacierised areas. Figure S2 illustrates the applied processing chain used to perform this coregistration. First, smooth stable reference areas are defined by masking out vegetation, water and glacier areas. The vegetation and water masks are derived from region wide cloud free Landsat 8 mosaics and using a normalized difference vegetation index (NDVI) threshold of 0.3 and a normalized difference water index (NDWI) threshold of 0.1. Additionally, a slope threshold of 15° (of the respective reference DEM) is applied. Thereafter, the TDX DEMs are bi-linearly vertically corrected for offsets to the reference DEM, which are measured on the defined stable regions. Subsequently, a horizontal coregistration between the reference DEM and the TDX DEMs is carried out following the widely used approach of Nuth and Kääb (2011). Afterwards, a second bi-linear vertical coregistration of the TDX DEMs to the reference DEM is run to reduce any biases that remain. Finally, the coregistered TDX DEMs are merged to a regional DEM mosaic, which include a date stamp for each grid cell.

To obtain elevation change rates $\Delta h/\Delta t$ of the respective study periods, the SRTM DEM and the TDX DEM mosaics are differentiated. The mean date of the eleven-day SRTM mission (2000-02-16) is assigned to the SRTM DEM. Since data voids in the SRTM DEM are filled with data from other sources (no date information available), the non-SRTM data values are masked out using the coverage information provided by LP DAAC NASA. Numerous studies have revealed that the glaciers in Peru are in general retreating (Section 1). Thus, the glacier inventory from the beginning of the respective observation period is employed to create surface elevation change maps for on- and off-glacier areas. The average regional and glacier-wise elevation change rates are obtained by integration of $\Delta h/\Delta t$ over the respective areas. Slopes steeper than 50° are rejected (5.7% of the glacier area in 2000), since major ice aggregation is quite unlikely there (avalanche slopes, backed up by field observations) and DEMs are less accurate on these steep slopes (Toutin, 2002). To account for data voids in the elevation change fields on glacierised areas, the measured $\Delta h/\Delta t$ values are area weighted based on the hypsometric area distribution using 100 m elevation bins in order to calculate regional mean values. This is one of the recommended methods to obtain regional estimates and provides reliable results for datasets with up to 60% voids (McNabb et al., 2019).

The average $\Delta h/\Delta t$ of individual glaciers is calculated according to McNabb et al. (2019) by using elevation bins of 10% of the glacier elevation range, if it is <500m, and bins of 50 m for glaciers with elevation ranges >500 m. A coverage of more than two-thirds of the elevation bins and <60% data gaps are used as a criterion for exclusion. Voids in the hypsometric $\Delta h/\Delta t$ distribution are filled by applying third order polynomial fit. Outliers in the respective elevation bins (regional and glacier-wise analysis) are sorted out using three times the normalized median absolute deviation (NMAD) (Brun et al., 2017). For all hypsometric analyses of elevation changes (SRTM to TDX, TDX to TDX), the void-filled SRTM DEM is utilized.

The uncertainties of the generated elevation change rates are assessed by evaluating the elevation change rates on non-vegetated stable off-glacier areas (water and vegetation masks, see above). The lowest and highest 2% quantiles of the change

rates are rejected to suppress the impact of processing artefacts and outliers. To account for the dependency of the offsets on

230   the slope (Figure 2 and S3 and S4), the deviations are binned in slope intervals of 5°. Remaining outliers are removed by employing a 3*NMAD filter for each slope bin. Finally, the area-weighted standard deviations σ_{AW} based on the offsets in off-glacier areas and the slope distribution in glacier areas are calculated.

Since we integrate elevation change information over the glacierised area, spatial auto correlation of the elevation change fields must be considered in the accuracy assessment. We estimated the uncertainty of the computed average elevation change

235   rates ($\sigma_{\Delta h/\Delta t}$) according to the approach of Rolstad et al. (2009):

$$\sigma_{\Delta h/\Delta t} = \sqrt{\frac{A_{cor}}{5A_{gl}}}\,\sigma_{AW} \qquad A_{gl} > A_{cor} \tag{1}$$

$$\sigma_{\Delta h/\Delta t} = \sigma_{AW} \qquad A_{gl} < A_{cor}$$

Where $A_{cor} = \pi * d_{cor}$ is the correlation area, A_{gl} is the analysed glacier area and σ_{AW} is the assessed accuracy of the elevation change rates (explained in the next paragraph). The correlation length (d_{cor}) is obtained by generating semivariograms with

240   100000 random samples of $\Delta h/\Delta t$ values on the off-glacier areas. A binning in 30 m distance intervals and a maximum distance of 20 km are applied. Spherical semivariogram functions are fitted to the data and an average correlation length of 387 m results from the analysed elevation change fields. Equation 1 is applied for each continuous glacierised area (icecap or connected glaciers) and the area-weighted average of the individual ice-covered areas is taken as the region wide $\sigma_{\Delta h/\Delta t}$.

The hypsometric extrapolation of elevation change information leads to an additional uncertainty that is hard to quantify. We

245   employed the approach of Berthier et al. (2014). A scaling factor (we selected a factor of 2) is applied to $\sigma_{\Delta h/\Delta t}$ for the area fraction with hypsometric extrapolation of $\Delta h/\Delta t$, in order to obtain the uncertainty of our region wide average elevation change rates $\delta_{\Delta h/\Delta t}$.

4.3   Mass balances

The geodetic mass balances $\Delta M/\Delta t$ of the analysed regions are computed according to Fountain et al. (1997) by multiplying the integrated elevation change rates by the average ice density (volume to mass conversion factor). We applied two density

250   scenarios. The first scenario follows the suggestion of Huss (2013) for alpine glaciers and we applied an average density (ρ) of 850 kg m^{-3}. For the second scenario, two different conversion factor of 600 kg m^{-3} and 900 kg m^{-3} are applied for ablation and accumulation areas, respectively (Kääb et al., 2012, Gardelle et al. 2012). The average ELA (see Table S3 and below) of each subregion is used to distinguish between both glacier sections. As revealed by Huss (2013), the conversion factor can vary strongly. Accordingly to his findings, we applied a uncertainty of ±300 kg m^{-3} for the conversion factor for observation

255   intervals shorter than 10 years and mass budgets lower than ±200 kg m^{-2} a^{-1} and an uncertainty of ±60 kg m^{-3} for all other cases (see also Braun et al., 2019). Mass budgets of individual glaciers are only calculated for the constant density scenario.

In order to estimate the accuracy of the geodetic mass balances, the following error contributions are considered:

- accuracy of the elevation change rates $\delta_{\Delta h/\Delta t}$

- accuracy of the glacier outlines δ_S

260   - uncertainty of the applied average ice density δ_ρ

- potential bias due to different SAR signal penetration $V_{pen}/\Delta t$

This leads to the following formula to calculate the error of $\Delta M/\Delta t$:

$$\delta_{\Delta M/\Delta t} = \sqrt{(\tfrac{\Delta M}{\Delta t})^2((\tfrac{\delta_{\Delta h/\Delta t}}{\tfrac{\Delta h}{\Delta t}})^2 + (\tfrac{\delta_S}{S})^2 + (\tfrac{\delta_\rho}{\rho})^2) + (\tfrac{V_{pen}}{\Delta t} * \rho)^2} \qquad (2)$$

The assessments of δ_S and $\delta_{\Delta h/\Delta t}$ are depicted in Section 4.1 and 4.2. The uncertainty contribution by potentially different SAR
265   signal penetration in the glacier surfaces is evaluated following the approach of Malz et al. (2018). No difference in the SAR
signal penetration in the ablation areas below the equilibrium line altitude (ELA) is assumed. These areas experience melt
throughout the year in the Tropical Andes (Kaser, 2001) and differences in the radar signal penetration in wet glacier surfaces
are small (Casey et al., 2016; Rossi et al., 2016; Ulaby et al., 1984). A linear increase of the penetration depth bias towards 5
m between the ELA and the highest peaks is employed in the accumulation areas to calculate V_{pen}. Depending on the applied
270   scenario volume to mass conversion factor of 850 kg m^{-3} or 600 kg m^{-3} is taken. The late summer snow line altitude (SLA)
derived from optical satellite images is a good proxy for the ELA in the Tropical Andes (Rabatel et al., 2012). Thus, the average
ELA in the study period for the subregions is estimated based on published ELA and SLA values. Table S3 provides an
overview of the considered ELA and SLA values. Uncertainties in the estimated ELA positions affect the penetration depth
bias estimation and thus the error budget. A sensitivity analysis of an ELA mismatch on the error budget is provided in Braun
275   et al. (2019). Specific mass balances are calculated according to the UNESCO Glossary of Glacier Mass Balance (Cogley et
al., 2011) by applying the average glacier area of each observation period (mean glacier extent with slopes <50°).

5   Results

5.1   Glacier inventory

The glacier outlines from 2000, 2013 and 2016 of some example mountain ranges from all 3 subregions are shown in Figure
S5. A clear recession of the glaciers in all subregions is obvious. The measured extents of the glaciers for all subregions and
time steps are presented in Table 1. Since cloud and snow cover do not allow for a complete coverage of subregion R1 and R2
280   in 2013 and no suitable SAR data cover the debris-covered ice areas in the Cordillera Blanca in 2013, a small fraction of the
glacier area (subregion R1: 2.1%; subregion R2: 4.4%) is mapped using imagery from 2014. For subregion R1, a nearly
complete mapping (99.5%) of the glacier areas in 2014 is possible. The obtained average area change rate between 2013 and
2014 at glaciers delimited in both years is employed to correct the area change measurement in subregion R1 for 2013 at
glaciers only delimited in 2014 and vice versa. In subregion R2, the change rate between 2013 and 2016 is applied to perform
285   a similar correction of the area change measurements in 2013. In total, ice covered areas of 1916.6±48.3 km² in 2000,
1571.9±43.1 km² in 2013 and 1368.1±45.5 km² are estimated for Peru. Based on the catchment divides of the RGI6.0, a
reduction in the number of glaciers from 1973 in 2000 to 1803 in 2016 is observed. The variations of the glacier count and

area in the subregions and of the whole country are summarized in Table 1 and 2. It should be noted, that the uncertainty of the area changes (Table 2) result from the uncertainty of the individual inventories (quadratic sum), assuming independence of the individual area measurements. The revealed area changes of individual glaciers in the different subregions and study periods are correlated with topographic parameters (glacier area, median elevation, mean aspect) and plotted in Figure 3 and S6-S13.

5.2   Elevation changes

The obtained unfiltered elevation change rates on ice-covered areas at some example mountain ranges are illustrated exemplary in Figure 4 and 5 for the periods 2000-2013 and 2013-2016, respectively. In the interval 2000-2013, a clear thinning of the lower glacier parts in the Cordillera Vilcanota and Apolobamba is observed. The glaciers in the Cordillera Blanca and Huayhuas show a more balanced pattern and Coropuna experienced thinning throughout most of its ice cap. An increase in the surface lowering rates at most mountain ranges is obvious in the interval 2013-2016. Only the ice caps in subregion R3 show reduced lowering rates. Since the TDX data in 2013 do not cover the whole glacier area in subregion R3, the voids are filled with TDX data from 2014. The glacier area covered by $\Delta h/\Delta t$ measurements using TDX data from 2014 amount to only 1.4% (glacier outlines from 2000). The impact of this void filling is considered negligible since the analysis uses change rates. The average measured and extrapolated surface elevation change rates of all subregions for different observation periods are listed in Table 2. The fraction of glacier area covered by $\Delta h/\Delta t$ measurements is lowest in subregion R1, when using the SRTM DEM as a reference (Table 2). Large data voids in the SRTM data lead to a partial coverage of only 46% of the ice covered area in subregion R1 in 2000 (61% in subregion R2, 89% in subregion R3). The amount of measurements on the glacierised areas clearly increases when deriving the elevation change solely from TDX datasets (Table 2). In the period 2013-2016, a coverage of up to 80%, 69% and 89% is obtained in subregion R1, R2 and R3, respectively. Since the differential InSAR approach is used to generate the TDX DEMs, the proportion of areas affected by phase-jumps in the unwrapped interferogram is small (~1% of the total glacier area). The major area affected by phase-jumps (at the Cordillera Vilcanota in 2016) is highlighted in Figure 5. Figures 4 and 5 indicate that the elevation change rates are altitude dependent. The hypsometric distributions of the measured elevation change rates and the respective ice covered areas are plotted in Figure 6, S14 and S15 for the each subregion in the interval 2000-2016. Surface lowering is found on areas below 5700m in subregion R1, 5800m in subregion R2 and 5900 m in subregion R3. Considerable positive elevation changes are observed in the higher reaches of the glaciers in subregion R1.

5.3   Mass balances

The geodetic mass balances derived from the elevation change information of the individual subregions are listed in Table 2. In total, a mass loss of -7.62±1.05 Gt or -9.18±1.10 Gt is found for Peru in the period 2000-2016, depending on the applied density scenario (Section 4.3). The mass loss rates show an increase between the observation periods 2000-2013 and 2013-2016. Only in subregion R3 is a slight reduction of the mass loss observed. The most prominent increase in glacier wastage is revealed in subregion R1. The mass budget changed from nearly stable conditions of 45±97 kg m^{-2} a^{-1} in 2000-2013 to a

10

specific mass loss rate of -752 ± 452 kg m^{-2} a^{-1} in 2013-2016 (2nd density scenario). The computed mass balances of individual glaciers in the different subregions and study periods are correlated with topographic parameters (glacier area, median elevation, mean aspect) and plotted in Figure 7 and S16-S20.

6   Discussion

6.1   Glacier retreat

We observed a dramatic recession of the glaciers throughout Peru of -29% (-548.5 ± 65.7 km²; -1.8 % a^{-1}) between 2000 and 2016. Our total mapped glacier extent of 1368.1 ± 44.5 km² in 2016 is comparable to the reported coverage of 1298.6 km² by the recent Peruvian Glacier Inventory (UGRH, 2014), considering that UGRH did not include the glacier areas of the Bolivian Cordillera Apolobamba (~70 km²). The glacier area mapped in the RGI6.0 amounts to 1602.96 km², which is in the range of our measurements for 2000 and 2013. A direct comparison is complex, since the RGI6.0 is a blended product with outlines discriminated between 2000 and 2009 in Peru. However, visual inspection of our outlines and the RGI6.0 revealed that numerous small glaciers (especially in the southern section of subregion R1 and throughout the whole subregion R3) mapped in the RGI6.0 are artefacts, which are caused most probably by temporary snow cover. This issue has already been mentioned in the RGI Technical Report (RGI Consortium, 2017). Thus, our glacier inventory of Peru in 2000 has 350 less features than the RGI6.0. By contrast, the Peruvian Glacier Inventory (UGRH, 2014) lists 2679 glaciers. This difference can be explained by the different basin delineations applied.

The comparison of our area measurement of 1916.6 ± 48.3 km² in 2000 and the 1st Peruvian Glacier Inventory (Hidrandina SA, 1989) in 1970 (2041.85 km²) results in a retreat of -7% (-139.9 km²; 0.2% a^{-1}). However, the area changes amounts to -23%, considering only glacierised Cordilleras, which were completely mapped in the 1st Peruvian Glacier Inventory (UGRH, 2014). Figure 8 illustrates the temporal evolution of the glacier area changes and highlights that Peru's glaciers have experienced long-term shrinkage since 1970 with increasing rates in recent years. This observed trend is in accordance with the findings of previous studies at individual mountain ranges. Silverio and Jaquet (2017) summarized area measurements of several studies in the Cordillera Blanca (subregion R1) and revealed an increase in the loss rate from about -5 km² a^{-1} between 1971 and 1996 towards -23 km² a^{-1} between 2014 and 2016. Burns and Nolin (2014) reported a ~3.5 times higher area loss rate in 2004-2010 compared to 1970-2003 in the Cordillera Blanca. Area loss rates of ~1.8 % a^{-1} (>50%) since 1975 are reported by the Instituto Geofisico del Peru (2010) and López-Moreno et al. (2014) for the Cordillera Huaytapallana, which is higher than our finding of -1.1 % a^{-1} in subregion R1 in the period 2000-2013. However, their study period includes strong El Niño events in the 1980/90s (Figure 8), which typically lead to increased glacier melt in the Tropical Andes (Wagnon et al., 2001). Retreat measurements in subregion R2 are carried out at the Cordillera Vilcanota (Hanshaw and Bookhagen, 2014; Salzmann et al., 2013; Veettil and Souza, 2017), the Cordillera Apolobamba (Cook et al., 2016; Veettil et al., 2017a), the Cordilleras Carabaya, Urubamba and Vilcabamba (Veettil et al., 2017d) and at glaciers draining into the Vilcanota-Urubamba basin (Drenkhan et al., 2018). All studies revealed significant glacier shrinkage since the 1980s with retreat rates in the range of -0.9 to -1.7 % a^{-1}.

These findings are comparable with our observed rate of -1.3 % a^{-1} in subregion R2 in the period 2000-2013. Drenkhan et al. (2018) revealed reduced shrinkage rates for 2010-2016 as compared to 2004-2014. This is contradictory to our observed strong

350 increase in glacier recession after 2013. They analysed only glaciers in the Vilcanota-Urubamba basin, of which most are south facing. We measured the highest retreat for glaciers facing north in subregion R2 in the period 2013-2016 (Figure S22) and only low retreat for south facing glaciers. Thus, different spatial extents and representativeness of topographic attributes in the analysed regions leads to the mismatch of the observed retreat trends. Moreover, this suggests that the representativeness of topographic settings needs to be considered when doing region wide upscaling of sampled glacier change measurements. At

355 the ice cap of the Coropuna volcano (subregion R3), various ice coverage estimates are available going back to 1955 (Peduzzi et al., 2010; Racoviteanu et al., 2007; Silverio and Jaquet, 2012; Ubeda, 2011; Veettil et al., 2016). The average loss rate of ~1.5 % a^{-1} (1955-2015) is lower than our estimated rate of -2.3 % a^{-1} for subregion R3 in the period 2000-2013. Besides differences in the study periods, we attribute this deviation to the fact that our estimate for subregion R3 includes numerous small glaciers located at lower altitudes (Figure S10). These glaciers are in general more sensitive to climate change (Francou

360 Bernard et al., 2003; Vuille et al., 2008) in comparison to the more elevated glaciers of the Coropuna volcano. Moreover, Veettil et al. (2016) discovered an increased retreat and uplift of the SLA after ~2000 at Coropuna's ice cap, supporting our findings.

For the period 2013-2016, we discovered a four times higher countrywide retreat rate compared to the period 2000-2013. The strongest increase is found in subregion R2, whereas in subregion R3 (only ~5% of total glacier area) the glacier area remained

365 quite stable after 2013. The increased retreat rates in subregions R1 and R2 after 2013 can be attributed to the strong ENSO activities in the years 2015/16. An average ONI of 0.42 is reported for 2013-2016 and the maximum ONI of 2.6 in December 2015 indicates distinct El Niño conditions. On the other hand, an average ONI of -0.17 is revealed for 2000-2013, indicating that La Niña conditions dominated this period. Since El Niño periods typically lead to increased glacier wastage in the Tropical Andes (e.g. Vuille et al., 2008; Wagnon et al., 2001) (Section 2), our observed increased shrinkage after 2013 can be attributed

370 to the ENSO activities in this period. This pattern fits also to the finding by Morizawa et al. (2013) (Condoriri Glacier, Bolivia) and Silvero and Jaquet (2017) (Cordillera Blanca, subregion R1). Both studies reported enhanced recession during El Niño events and even area gains during La Niña epochs. The latter study also discovered a linear relation between glacier retreat and ONI (R²=0.8) and reports an change rate of -5% a^{-1} for 2014-2016 that is equal to our change rate at subregion R1 for 2013-2016. Moreover, the glaciers in the Tropical Andes are in average the thinnest worldwide (Farinotti et al. 2019).

375 Therefore, the increased melt will lead to more pronounced changes in glacier area as compared to other glacier region. The stagnation of the glacier retreat in subregion R3 in the interval 2013-2016 is difficult to explain. During the strong El Niño in 1997/98, increased precipitation was observed at the Coropuna volcano in subregion R3 (Herreros et al., 2009; Silverio and Jaquet, 2012), whereas, El Niño usually leads to reduced precipitation rates. Veettil et al. (2016) reported positive precipitation anomalies after 2011 and clearly negative anomalies in the period 2009-2011 for the Coropuna volcano. However, the total

380 precipitation data from ERA-Interim indicate lower precipitation rates after 2013 (Figure S24) and do not clearly indicate an increase in precipitation during El Niño 1997/98. Since the small glacier areas in subregion R3 cover mainly volcano peaks,

the revealed precipitation values from the spatially coarse ERA-Interim data do not necessarily reflect the local precipitation pattern at the prominent, high altitude volcano peaks. Additionally, the mean glacier altitude in 2013 shifted ~100 m above the ELA (Figure S25), whereas the mean glacier altitude in 2000 was nearly similar to the ELA (Figure S15). A significant temporary snow cover at the non-glacierised Cordillera Barroso (subregion R3, close to the boarder to Bolivia) was observed during the dry seasons in 2015 and 2016 (Lèon et al. 2019), which fits to the suggested increased precipitation at high elevations after 2013. Moreover, snowfall events during try season strongly affect the glacier albedo and thus lead to reduced ablation. However, the temporary snow cover during dry season 2016 in subregion R3 might have also affected the mapping of the glacier outlines. Albeit, only imagery with no or only minimal snow coverage is selected, it is quite likely that some remaining snow cover was located at the glacierised peaks, leading to a slightly larger glacier area in 2016 as compared to 2013. This bias is not quantifiable and certainly within the range of applied uncertainty. Thus, we conclude that the glacier area kept nearly stable after 2013 in subregion R3 and attribute this to the allocation of the remaining ice at higher altitudes and increased precipitation, especially during the dry season, even though a strong El Niño event occurred in this period.

The analysis of area fluctuations of individual glaciers revealed in all three subregions indicates higher recession for glaciers with lower median elevation and for small glaciers (Figure 3 and S6-S13). This is in accordance with findings reported in previous studies (e.g. Kaser and Osmaston, 2002; Mark and Seltzer, 2005; Ramirez et al., 2001). Small glaciers have in general a more narrow altitude range as compared to larger glaciers, which can maintain the ELA below the maximum glacier elevation. A rise in SLA (a proxy of the ELA in the Tropical Andes, Section 4.3) is observed throughout the Peruvian Andes by various studies (Hanshaw and Bookhagen, 2014; López-Moreno et al., 2014; McFadden et al., 2011; Veettil et al., 2016, 2017d, 2017c). This corresponds to our observed retreat pattern. Figure 3 and S6-S13 suggest that glaciers with slopes facing on average in the south/south-west direction experienced in general higher relative retreats. The total amount of lost glacier area repeats this general pattern (Figure S21-23). This can be attributed to the fact that more low lying, small glaciers with mean aspects facing southwards still exist (Figure 3 and S6-S13). Higher retreat rates in general were observed for north-orientated glaciers before 2000 (Veettil et al., 2017a; Veettil, 2018), leading already to the disappearance of small north-facing glaciers before the start of our observation periods.

In total, we discovered that 177 glaciers disappeared in our observation period, of which most disappeared after 2013 and were south facing (Table 1 and Figure S11-S13). At the Artesonraju Glacier in the Cordillera Blanca (subregion R1), Vuille et al. (2018) projected an uplift of the ELA by 300-700 m until 2100 based on the CMIP 5 scenarios RCP 4.5 and 8.5. Thus, the proceeding climate change will lead to the further disappearance of numerous small low-lying glaciers in the Tropical Andes within the next decades, as predicted by Ramirez et al. (2001) and Huh et al. (2017).

The gain and formation of proglacial lakes are consequences of glacier recession (Cook and Quincey, 2015), and increases the GLOF risk of downstream areas. Veettil et al. (2017a) discovered an increase in the number of glacial lakes from 697 to 903 in the Cordillera Apolobamba and Carabaya between 1985 and 2015. In the Cordillera Vilcanota, Hanshaw and Bookhagen (2014) observed stable or increasing extents in 77% of the lakes connected to glacial watersheds. Colonia et al. (2017) compiled an inventory of 201 potential future glacier lakes based on modelled glacier bed overdeepenings. Considering the revealed

13

findings by this study as well as previously reported values and projections, a further region wide monitoring of glacier retreat and lake development is highly advisable to identify potential GLOF risks in the Tropical Andes, as also suggested by Cook et al. (2016).

6.2 Surface elevation changes and mass balances

The average countrywide glacier surface elevation change between 2000 and 2016 amounts to -0.359±0.068 m/a, which corresponds to a specific mass budget of -296±41 kg m^{-2} a^{-1} or -357±43 kg m^{-2} a^{-1} depending on the applied density scenario. The 2nd density scenario leads to 8-21% lower country wide mass balances. As pointed out by Kääb et al. (2012), this scenario is suitable for glacier with no *dh/dt* due to ice dynamics and when *dh/dt* is clearly driven by melt or increased accumulation. Since, these conditions are typical for the Peruvian glaciers (see Section 1 and further down), we used the results of 2nd density scenario for further discussion and analyses. Whereas, the results from the 1st scenario provide suitable information for comparison with other studies. Moreover, using the 2nd scenario reduces the potential bias by the SAR signal penetration depth differences (Section 3) on the mass budget by ~40% as compared to the 1st scenario. A computation of individual glacier mass balances using the 2nd scenario is not performed due to the lack of ELA information on glacier-scales.

The highest average surface lowering is revealed for subregion R1 in the period 2013-2016 (Table 2). However, the stable surface elevations before 2013 in subregion R1 suppress the long-term average value. The nearly balanced budget contradicts the observed glacier retreat of -15% in subregion R1 in the interval 2000-2013 at first glance. The mean surface elevation change in the retreat areas amounts to -0.28 m/a, clearly indicating mass loss in the deglacierised areas. However, elevation gain is found at high altitudes. The more La Niña-like conditions of the ENSO in the period 2000-2013 (Section 6.1) and an increase in precipitation in this region due to stronger upper-tropospheric easterlies (Schauwecker et al., 2017) has most probably led to higher accumulation rates. ERA-Interim reanalysis data also show an increase in total precipitation in this period, especially around 2007 (La Niña event). Thus, the accumulation gain in the upper reaches balanced the ice losses at the termini, even though temperatures increased (Schauwecker et al., 2017). In all subregions an increase in temperature is found in the reanalysis data for 2000-2013, but the strongest positive precipitation anomaly is found in subregion R1 (Figure S24 and S26). This explains the mass losses in subregions R2 and R3 in this period.

Skin temperature was still above the long-term average in subregion R1 and R2 after 2013 (Figure S26). The downward surface thermal radiation shows an increase in subregion R1 (Figure S27), whereas total precipitation decreased in subregion R2 and remained nearly stable in subregion R1 (Figure S24). Those climatic variations enhance the ablation and facilitate a positive feedback that further increase the glacier melt. The higher temperature as well as reduced and delayed precipitation, that are typical during El Niño, lead to liquid precipitation in the ablation regions and a reduced glacier albedo, enhancing the short-wave radiation absorption (e.g. Vuille et al. 2018, Maussion et al. 2015). Thus, the climatic variations explain the more negative mass balances in both subregions in the period 2013-2016, which also correlate with the strong El Niño activities in this interval (Figure 8).

Only at subregion R3 did the thinning rate reduce after 2013, although El Niño conditions dominated. We attribute this, like the stable glacier area, to higher precipitation rates, especially during dry season, at the ice capped volcanos and the allocation of the remaining ice masses at high elevations (Section 6.1 for more details). Moreover, the revealed spatial pattern of mass balances after 2013, with highest mass loss rates at the northern most subregion R1 (Table 2), matches the observed trend of higher river runoff towards northern Peru during strong El Niño events (Casimiro et al., 2012, 2013).

The analysis of the mass balance of individual glaciers and topographic parameters in subregions R2 and R3 reveals a trend towards higher mass losses for glaciers facing north/north-east in the period 2000-2016 (Figure 7, S16 and S17). This trend agrees with observations by Soruco et al. (2009a) in the Bolivian southern wet outer tropics. In the interval 2000-2016, no clear dependency of the specific glacier mass balances on the median elevation or aspect is obvious in subregion R1 (Figure 7). However, Figure 5 suggests a trend towards higher surface lowering rates on the western slopes of the Cordillera Blanca in the period 2013-2016. The subregion-wide analysis of glacier elevation changes in dependency to aspect does not reveal any clear trend (Figure S28), however, when analysing only the Cordillera Blanca an east to west gradient is obvious (Figure S29). We attribute this to the changed precipitation pattern during El Niño. Higher precipitation rates are typically found on east-facing slopes at the Cordillera Blanca, fed by moist air from the Amazon basin (Garreaud et al., 2009). However, during El Niño the westward flow of the moist air is hampered by stronger westerlies (Vuille, 2013), which increases the precipitation gradient across the Cordillera Blanca.

Long-term glaciological mass balance measurements are only available for two glaciers (WGMS, n.d.). For the Artesonraju and Yanamarey glaciers, both located in subregion R1, average mass budgets of -911 kg m^{-2} a^{-1} and -1.491 km/m² a^{-1} (2013-2016) are revealed from field measurements, whereas we observed -962±228 kg m^{-2} a^{-1} and -3167±2317 kg m^{-2} a^{-1}, respectively. Both methods show higher loss rates for the Yanamarey Glacier as compared to the Artesonraju Glacier. The deviation of ~50% between both approaches at Yanamarey Glacier (overlap within the error range) can be partly attributed to different observation intervals and basin delinations. Moreover, glaciological mass balance measurements are typically based on some stake measurements in the lower, often most accessible, ablation zone and only a few measurements in the accumulation region. At the Zongo Glacier, Bolivia, Soruco et al. (2009b) performed a comparison of different mass balance methods (glaciological, hydrological and geodetic) and revealed a strong offset in the glaciological mass balance estimates. The authors suggest that the limited number of field measurement points is not representative of the whole glacier and that the interpolation between the measurement sites can bias glacier wide specific mass balance information. On the other hand, to obtain glacier wide mass balance estimates using the geodetic method, there is interpolation over data voids in the elevation change fields needed (in our case we used the hypsometric elevation change distribution). Thus, we attribute the offset between the results from both methods to uncertainties due to interpolation, spatial sampling and different observation periods.

The correlation of the annual glaciological measurements with the average ONI of the respective observation periods indicates a trend towards increased mass loss and higher ELA during El Niño conditions (Figure S30). These tendencies fit to the observations by Silvero and Jaquet (2017) and Morizawa et al. (2013) (see Section 6.1) and support our revealed correlation between the increased glacier wastage in the period 2013-2016 and the strong El Niño event during this period.

Since the highest density of glaciological point measurements are collected at the lowest section at both glacier and considering the observation of Soruco et al. (2009) at Zongo Glacier, Bolivia, that the terminus region strongly dominates the mass balance variations of a tropical glacier, we did an analysis of the glaciological mass balance at regions below 4900 m a.s.l. and 5000 m a.s.l. at Yanamarey and Artesonraju glaciers, respectively. A trend toward increased mass losses after 2011 is obvious (Figure S31, unfortunately the data at Yanamarey Glacier for the period 2009-2011 were incomplete), fitting to the revealed more negative geodetic mass balances after 2013. Moreover, the most negative values are derived for the period 2015-2016, which also supports our suggestion, that ENSO force the increased glacier wastage after 2013. The comparison between the geodetic and the average glaciological measurements at the terminus regions in the period 2013-2016 revealed a good agreement of both methods at Yanamarey Glacier (average glaciological: -3152 kg m^{-2}a^{-1}, geodetic: -3164 kg m^{-2}a^{-1}), whereas at Artesonraju Glacier, the geodetic measurements indicate higher mass loss (average glaciological: -4206 kg m^{-2}a^{-1}, geodetic: -2696 kg m^{-2}a^{-1}). This difference can be partly attributed to the different glacier basin definitions and slightly different observation intervals, but also to limitations of the individual methods, as discussed above.

In subregion R1, Huh et al. (2017) derived volume losses ranging from -0.019 km^3 to -0.150 km^3 at six glaciers in the Cordillera Blanca from various elevation datasets in the period 1962-2008. This ice depletion corresponds to surface lowering rates of -0.20 m/a to -1.4 m/a. Mark and Seltzer (2005) reported lowering rates ranging from -0.14 to -0.59 m/a for three glaciers at the Nevado Queshque (Cordillera Blanca, subregion R1) in the interval 1962-1999. The findings of both studies are in the range of our revealed elevation change rates for subregion R1 of -0.208±0.065 m/a and -1.067±0.273 m/a in the periods 2000-2016 and 2013-2016, respectively.

In subregion R2, Salzmann et al. (2013) estimated an ice volume loss in the Cordillera Vilcanota of ~40-45% between 1962 and 2006 based on ice thickness derived from glacier inventory parameters and thickness-volume scaling. The authors pointed out that nearly all ice loss occurred after 1985, leading to a lowering rate of about -0.39 m/a for the period 1985-2006. This value is similar to our measured average surface lowering in subregion R3 of -0.440±0.069 m/a in the interval 2000-2013.

At the Coropuna volcano in subregion R3, Racoviteanu et al. (2007) measured an average glacier surface lowering of -5 m (-0.1 m/a) based on a SRTM DEM and digitizing of a topographic map from 1955. Peduzzi et al. (2010) calculated a mean surface lowering of -0.2±0.3 m/a for the period 1955-2000/02. Our revealed average surface lowering of -0.44±0.045 m/a at the ice cap of the Coropuna volcano indicates an increased glacier wastage after 2000, which correlates with the increase in glacier retreat and SLA uplift observed by Veettil et al. (2016) since 2000.

The continent-wide surface mass balance simulation by Mernild et al. 2017 revealed an average mass change of -1230±690 kg m^2 a^{-1} for the Andes north of 27°S in the epoch 2000-2014, which is much higher than our country-wide average of -169±43 kg m^2 a^{-1} for the period 2000-2013. This large offset can only be partly explained by the different study domains, time intervals and glacier inventories applied, and could be cause by limitations in the applied statistical downscaling of global circulation data.

On the countrywide scale, we observed ~19 % less mass loss than Braun et al. (2019) (Region 02-04) in the period 2000-2012/13 (1st density scenario). However, their analysis also includes the glacier areas in Bolivia, like the Cordillera Real, where

515 significant glacier wastage is reported (e.g. Soruco et al., 2009a), leading to higher average mass loss rates. The change rates of subregion R1 and R2 in the period 2000-2012/13 and the results of Braun et al. (2019) in Region 02 and 03 show good agreement, even though they are based on different glacier inventories. However, we computed more negative mass budgets in subregion R3 as compared to Braun et al. (2019) (Region 04). This can be partly explained by the differences in the region delineation. Braun et al. (2019) included the few ice-covered volcanoes in south-west Bolivia. However, a more considerable

520 reason for this offset is the fact that we found the highest amount of misclassified ice covered areas in the RGI 6.0 in this subregion (Section 6.1). This explains the bias toward lower mass loss rates in the results of Braun et al. (2019), who measured surface elevation changes based on the RGI 6.0. In a continent wide analysis of geodetic mass budgets, like that of Braun et al. (2019), it is beyond the scope of the studies to map glacier outlines fitting to the whole elevation database as well. However, the revealed offset suggests the inaccuracy caused by imprecise glacier outlines and highlights the need for large-scale

525 temporally consistent glacier outlines.

Gardner et al. (2013) carried out a comprehensive worldwide estimate of the glacier contribution to sea level rise. They computed a mass budget of -1080±360 kg m^{-2} a^{-1} (2003-2009) at the "low latitudes" (RGI region definition) by means of the extrapolation of glaciological measurements. A nearly similar value of -1.03 ± 0.83 m w.e. a^{-1} (-1030±830 kg m² a^{-1}) is revealed by Zemp et al. (2019) by upscaling of glaciological and geodetic mass balances for the period 2006-2016. Both studies reported

530 ice loss rate that are about three times higher than our countrywide average of -296±41 kg m^{-2} a^{-1} (2000-2016). However, they are based on very few measurements (e.g. <2% spatial coverage for Zemp et al. 2019) in this region, resulting to the large uncertainties. Moreover, the representativeness of the settings of the sampled glaciers, which is not assessed, can also strongly influence region wide estimates as discussed in Section 6.1. A comparison with GRACE measurements by Jacob et al. (2012) is also difficult, since their spatial domain covers the whole of South America, only excluding Patagonia. Thus, the mass

535 balance of the Peruvian glaciers cannot be disentangled from their results. These factors depict the limitations of using present global mass balance estimates at the country or even mountain range level.

The above-mentioned global or country-wide estimates do not cover multiple periods and thus do not provide any information on temporal variability of the mass balances. Our analysis reveals strong temporal variations in the glacier changes that correlate with changing climate conditions and specific climatic events. These findings underline that mono-temporal analysis,

540 especially when using short time intervals, can be biased by short-term climate anomalies like El Niño and highlights the need for further monitoring of the proceeding glacier recession in the Tropical Andes.

7 Conclusions

The glaciers throughout Peru are strongly affected by changing climatic conditions, leading to considerable ice losses. In this comprehensive study we revealed a glacier recession of -548.5±65.7 km² (-29%) in the period 2000-2016 and negative regional mass budgets of up to -752±452 kg m^{-2} a^{-1} (northern wet outer tropics; 2013-2016). A strong increase in the countrywide mass

545 and area loss rates from -169±43 kg m^{-2} a^{-1} and -1.4% a^{-1} in the period 2000-2013 to -660±178 kg m^{-2} a^{-1} and -4.3 % a^{-1} in the

interval 2013-2016 is shown. This amplified glacier wastage can be attributed to the strong El Niño in 2015/16. Spatial and temporal differences of the change rates of the studied subregions correlate with skin temperature and total precipitation trends derived from ERA-Interim reanalysis data and reported regional climatic variations. The analysis of area changes of individual glaciers indicates that the highest relative area change rates are found for low lying and small glaciers, validating the prediction
550   of the disappearance of numerous small glaciers located at low altitudes in the Tropical Andes.

Our results provide the first multi-temporal region wide and spatially detailed analysis covering all glacierised areas in Peru, providing fundamental data for projecting future glacier changes, water resource management schemes and further glacier monitoring. The observed changes highlight the dramatic progression of glacier recession throughout Peru, which will lead to considerable socio-economic issues in this region. The increasing GLOF risk, due to the gain and formation of glacial lakes is
555   just one aspect. The future contribution of glacier meltwater to the regional runoff puts the continuous water availability for irrigation, mining, hydropower generation and drinking water supply, especially during dry season, at risk. Therefore, we highly advocate resuming and further extending the glacier monitoring in the Tropical Andes, not solely to gain scientific knowledge, but also to provide important information for local authorities and decision-makers regarding water resource management and civil protection.

560   **Author Contributions:** TS designed and led the study, processed and analysed the data and wrote the manuscript. TS, PM and CS developed jointly the analysis routines for elevation change and mass balance computations. SL performed the SAR coherence computations. AC contributed to the interpretation of the data and provided field measurements. MB initiated and supervised the project. All authors revised the manuscript.

Data and materials availability: Elevation change fields will be available via the World Data Center PANGAEA operated by AWI Bremerhaven after acceptance of the manuscript. Glacier area information and glacier-specific results will also be made
575   available through submission to the World Glacier Monitoring Service and GLIMS.

8   References

Atwood, D. K., Meyer, F. and Arendt, A.: Using L-band SAR coherence to delineate glacier extent, Canadian Journal of Remote Sensing, 36(sup1), S186–S195, doi:10.5589/m10-014, 2010.

Baraer, M., Mark, B. G., McKenzie, J. M., Condom, T., Bury, J., Huh, K.-I., Portocarrero, C., Gómez, J. and Rathay, S.: Glacier recession and water resources in Peru's Cordillera Blanca, Journal of Glaciology, 58(207), 134–150, doi:10.3189/2012JoG11J186, 2012.

Berthier, E., Vincent, C., Magnússon, E., Gunnlaugsson, Á. Þ., Pitte, P., Le Meur, E., Masiokas, M., Ruiz, L., Pálsson, F., Belart, J. M. C. and Wagnon, P.: Glacier topography and elevation changes derived from Pléiades sub-meter stereo images, The Cryosphere, 8(6), 2275–2291, doi:10.5194/tc-8-2275-2014, 2014.

Braun, M., Malz, P., Sommer, C., Farias, D., Sauter, T., Casassa, G., Soruco, A., Skvarca, P. and Seehaus, T.: Constraining glacier elevation and mass changes in South America, Nature Climate Change, 9, 130-136, doi:10.1038/s41558-018-0375-7, 2019.

Brun, F., Berthier, E., Wagnon, P., Kääb, A. and Treichler, D.: A spatially resolved estimate of High Mountain Asia glacier mass balances from 2000 to 2016, Nature Geoscience, 10(9), 668, doi:10.1038/ngeo2999, 2017.

Burns, P. and Nolin, A.: Using atmospherically-corrected Landsat imagery to measure glacier area change in the Cordillera Blanca, Peru from 1987 to 2010, Remote Sensing of Environment, 140, 165–178, doi:10.1016/j.rse.2013.08.026, 2014.

Carey, M.: In the Shadow of Melting Glaciers: Climate Change and Andean Society, Oxford University Press., 2010.

Casey, J. A., Howell, S. E. L., Tivy, A. and Haas, C.: Separability of sea ice types from wide swath C- and L-band synthetic aperture radar imagery acquired during the melt season, Remote Sensing of Environment, 174, 314–328, doi:10.1016/j.rse.2015.12.021, 2016.

Casimiro, W. S. L., Ronchail, J., Labat, D., Espinoza, J. C. and Guyot, J. L.: Basin-scale analysis of rainfall and runoff in Peru (1969–2004): Pacific, Titicaca and Amazonas drainages, Hydrological Sciences Journal, 57(4), 625–642, doi:10.1080/02626667.2012.672985, 2012.

Casimiro, W. S. L., Labat, D., Ronchail, J., Espinoza, J. C. and Guyot, J. L.: Trends in rainfall and temperature in the Peruvian Amazon–Andes basin over the last 40 years (1965–2007), Hydrological Processes, 27(20), 2944–2957, doi:10.1002/hyp.9418, 2013.

Center, N. C. P.: NOAA's Climate Prediction Center, [online] Available from: http://origin.cpc.ncep.noaa.gov/products/analysis_monitoring/ensostuff/ONI_v5.php (Accessed 20 April 2018), n.d.

Cogley, J. G., Hock, R., Rasmussen, L. A., Arendt, A. A., Bauder, A., Braithwaite, R. J., Jansson, P., Kaser, G., Möller, M., Nicholson, L. and Zemp, M.: Glossary of Glacier Mass Balance and Related Terms. IHP-VII Technical Documents in Hydrology No. 86, IACS Contribution No. 2, UNESCO-IHP, Paris., Polar Record, 48(04), doi:10.1017/S0032247411000805, 2011.

Colonia, D., Torres, J., Haeberli, W., Schauwecker, S., Braendle, E., Giraldez, C. and Cochachin, A.: Compiling an Inventory of Glacier-Bed Overdeepenings and Potential New Lakes in De-Glaciating Areas of the Peruvian Andes: Approach, First Results, and Perspectives for Adaptation to Climate Change, Water, 9(5), 336, doi:10.3390/w9050336, 2017.

Cook, S. J. and Quincey, D. J.: Estimating the volume of Alpine glacial lakes, Earth Surface Dynamics, 3(4), 559–575, doi:https://doi.org/10.5194/esurf-3-559-2015, 2015.

Cook, S. J., Kougkoulos, I., Edwards, L. A., Dortch, J. and Hoffmann, D.: Glacier change and glacial lake outburst flood risk in the Bolivian Andes, The Cryosphere, 10(5), 2399–2413, doi:10.5194/tc-10-2399-2016, 2016.

Dee, D. P., Uppala, S. M., Simmons, A. J., Berrisford, P., Poli, P., Kobayashi, S., Andrae, U., Balmaseda, M. A., Balsamo, G., Bauer, P., Bechtold, P., Beljaars, A. C. M., van de Berg, L., Bidlot, J., Bormann, N., Delsol, C., Dragani, R., Fuentes, M., Geer, A. J., Haimberger, L., Healy, S. B., Hersbach, H., Hólm, E. V., Isaksen, L., Kållberg, P., Köhler, M., Matricardi, M., McNally, A. P., Monge-Sanz, B. M., Morcrette, J.-J., Park, B.-K., Peubey, C., de Rosnay, P., Tavolato, C., Thépaut, J.-N. and Vitart, F.: The ERA-Interim reanalysis: configuration and performance of the data assimilation system, Quarterly Journal of the Royal Meteorological Society, 137(656), 553–597, doi:10.1002/qj.828, 2011.

Drenkhan, F., Guardamino, L., Huggel, C. and Frey, H.: Current and future glacier and lake assessment in the deglaciating Vilcanota-Urubamba basin, Peruvian Andes, Global and Planetary Change, 169, 105–118, doi:10.1016/j.gloplacha.2018.07.005, 2018.

Drenkhan, F., Huggel, C., Guardamino, L., Haeberli, W., 2019. Managing risks and future options from new lakes in the deglaciating Andes of Peru: The example of the Vilcanota-Urubamba basin. Science of The Total Environment 665, 465–483. https://doi.org/10.1016/j.scitotenv.2019.02.070

Farinotti, D., Huss, M., Fürst, J.J., Landmann, J., Machguth, H., Maussion, F., Pandit, A., 2019. A consensus estimate for the ice thickness distribution of all glaciers on Earth. Nat. Geosci. 12, 168. https://doi.org/10.1038/s41561-019-0300-3

Favier, V., Wagnon, P. and Ribstein, P.: Glaciers of the outer and inner tropics: A different behaviour but a common response to climatic forcing, Geophys. Res. Lett., 31(16), L16403, doi:10.1029/2004GL020654, 2004.

Fountain, A. G., Krimmel, R. M., Trabant, D. and Geological Survey (U.S.): A strategy for monitoring glaciers, U.S. G.P.O. ; Free on applications to the U.S. Geological Survey, Information Services, [Washington]; Denver, CO., 1997.

Francou Bernard, Vuille Mathias, Wagnon Patrick, Mendoza Javier and Sicart Jean-Emmanuel: Tropical climate change recorded by a glacier in the central Andes during the last decades of the twentieth century: Chacaltaya, Bolivia, 16°S, Journal of Geophysical Research: Atmospheres, 108(D5), doi:10.1029/2002JD002959, 2003.

Gardelle, J., Berthier, E., Arnaud, Y., 2012. Slight mass gain of Karakoram glaciers in the early twenty-first century. Nat. Geosci. 5, 322–325. https://doi.org/10.1038/ngeo145

Gardner, A. S., Moholdt, G., Cogley, J. G., Wouters, B., Arendt, A. A., Wahr, J., Berthier, E., Hock, R., Pfeffer, W. T., Kaser, G., Ligtenberg, S. R. M., Bolch, T., Sharp, M. J., Hagen, J. O., Broeke, M. R. van den and Paul, F.: A Reconciled Estimate of Glacier Contributions to Sea Level Rise: 2003 to 2009, Science, 340(6134), 852–857, doi:10.1126/science.1234532, 2013.

Garreaud, R. D., Vuille, M., Compagnucci, R. and Marengo, J.: Present-day South American climate, Palaeogeography, Palaeoclimatology, Palaeoecology, 281(3–4), 180–195, doi:10.1016/j.palaeo.2007.10.032, 2009.

Georges, C.: 20th-Century Glacier Fluctuations in the Tropical Cordillera Blanca, Perú, Arctic, Antarctic, and Alpine Research, 36(1), 100–107, 2004.

GLIMS algorithm working group: GLIMS algorithm working group, [online] Available from: http://glims.colorado.edu/algorithms/algor.html#Anchor-3800 (Accessed 5 April 2018), n.d.

Hanshaw, M. N. and Bookhagen, B.: Glacial areas, lake areas, and snow lines from 1975 to 2012: status of the Cordillera Vilcanota, including the Quelccaya Ice Cap, northern central Andes, Peru, The Cryosphere, 8(2), 359–376, doi:10.5194/tc-8-359-2014, 2014.

Hastenrath, S. and Ames, A.: Recession of Yanamarey Glacier in Cordillera Blanca, Peru, during the 20th century, Journal of Glaciology, 41(137), 191–196, doi:10.3189/S0022143000017883, 1995.

Herreros, J., Moreno, I., Taupin, J.-D., Ginot, P., Patris, N., Angelis, M. D., Ledru, M.-P., Delachaux, F. and Schotterer, U.: Environmental records from temperate glacier ice on Nevado Coropuna saddle, southern Peru, in Advances in Geosciences, vol. 22, pp. 27–34, Copernicus GmbH., 2009.

Hidrandina SA: Inventario de Glaciares del Perú, 1989.

Hoffmann, D.: Participatory Glacier Lake Monitoring in Apolobamba Protected Area. A Bolivian Experience « Journal of Sustainability Education, [online] Available from: http://www.jsedimensions.org/wordpress/content/participatory-glacier-lake-monitoring-in-apolobamba-protected-area-a-bolivian-experience_2012_03/ (Accessed 22 October 2018), 2012.

Huh, K. I., Mark, B. G., Ahn, Y. and Hopkinson, C.: Volume change of tropical Peruvian glaciers from multi-temporal digital elevation models and volume–surface area scaling, Geografiska Annaler: Series A, Physical Geography, 99(3), 222–239, doi:10.1080/04353676.2017.1313095, 2017.

Huss, M.: Density assumptions for converting geodetic glacier volume change to mass change, The Cryosphere, 7(3), 877–887, doi:10.5194/tc-7-877-2013, 2013.

Instituto Geofisico del Peru, D. R. W.: Cambio climatico en la cuenca del rio mantaro, , 260, 2010.

Jacob, T., Wahr, J., Pfeffer, W. T. and Swenson, S.: Recent contributions of glaciers and ice caps to sea level rise, Nature, 482(7386), 514–518, doi:10.1038/nature10847, 2012.

Kääb, A., Berthier, E., Nuth, C., Gardelle, J., Arnaud, Y., 2012. Contrasting patterns of early twenty-first-century glacier mass change in the Himalayas. Nature 488, 495–498. https://doi.org/10.1038/nature11324

Kaser, G.: Glacier-climate interaction at low latitudes, Journal of Glaciology, 47(157), 195–204, doi:10.3189/172756501781832296, 2001.

Kaser, G. and Osmaston, H.: Tropical Glaciers, Cambridge University Press., 2002.

Kaser, G., Juen, I., Georges, C., Gómez, J. and Tamayo, W.: The impact of glaciers on the runoff and the reconstruction of mass balance history from hydrological data in the tropical Cordillera Blanca, Perú, Journal of Hydrology, 282(1), 130–144, doi:10.1016/S0022-1694(03)00259-2, 2003.

Léon, H., Loarte, E., Medina, K., Dávila, L., Rabatel, A., Muñoz, R., Rastner, P., Frey, H., 2019. Multi-temporal snow cover analysis with MODIS data in the Cordillera Barroso, Peru, in: EGU2019-10368. Presented at the EGU General Assembly 2019, Vienna, p. 1.

Lippl, S., Vijay, S. and Braun, M.: Automatic delineation of debris-covered glaciers using InSAR coherence derived from X-, C- and L-band radar data: a case study of Yazgyl Glacier, Journal of Glaciology, 1–11, doi:10.1017/jog.2018.70, 2018.

Lopez, P., Chevallier, P., Favier, V., Pouyaud, B., Ordenes, F. and Oerlemans, J.: A regional view of fluctuations in glacier length in southern South America, Global and Planetary Change, 71(1–2), 85–108, doi:10.1016/j.gloplacha.2009.12.009, 2010.

López-Moreno, J. I., Fontaneda, S., Bazo, J., Revuelto, J., Azorin-Molina, C., Valero-Garcés, B., Morán-Tejeda, E., Vicente-Serrano, S. M., Zubieta, R. and Alejo-Cochachín, J.: Recent glacier retreat and climate trends in Cordillera Huaytapallana, Peru, Global and Planetary Change, 112, 1–11, doi:10.1016/j.gloplacha.2013.10.010, 2014.

Malz, P., Meier, W., Casassa, G., Jaña, R., Skvarca, P. and Braun, M. H.: Elevation and Mass Changes of the Southern Patagonia Icefield Derived from TanDEM-X and SRTM Data, Remote Sensing, 10(2), 188, doi:10.3390/rs10020188, 2018.

Mark, B. G. and Seltzer, G. O.: Evaluation of recent glacier recession in the Cordillera Blanca, Peru (AD 1962–1999): spatial distribution of mass loss and climatic forcing, Quaternary Science Reviews, 24(20–21), 2265–2280, doi:10.1016/j.quascirev.2005.01.003, 2005.

Maussion, F., Gurgiser, W., Großhauser, M., Kaser, G., Marzeion, B., 2015. ENSO influence on surface energy and mass balance at Shallap Glacier, Cordillera Blanca, Peru. The Cryosphere 9, 1663–1683. https://doi.org/10.5194/tc-9-1663-2015

McNabb, R., Nuth, C., Kääb, A., Girod, L., 2019. Sensitivity of glacier volume change estimation to DEM void interpolation. The Cryosphere 13, 895–910. https://doi.org/10.5194/tc-13-895-2019

McFadden, E. M., Ramage, J. and Rodbell, D. T.: Landsat TM and ETM+ derived snowline altitudes in the Cordillera Huayhuash and Cordillera Raura, Peru, 1986–2005, The Cryosphere, 5(2), 419–430, doi:10.5194/tc-5-419-2011, 2011.

Mernild, S.H., Liston, G.E., Hiemstra, C., Wilson, R., 2017. The Andes Cordillera. Part III: glacier surface mass balance and contribution to sea level rise (1979–2014). International Journal of Climatology 37, 3154–3174. https://doi.org/10.1002/joc.4907

Morizawa, K., Asaoka, Y., Kazama, S., Gunawardhana, L.N., 2013. Temporal glacier area changes correlated with the El Niño/La Niña Southern Oscillation using satellite imagery. Hydrol. Res. Lett. 7, 18–22. https://doi.org/10.3178/hrl.7.18

NASA JPL: NASA Shuttle Radar Topography Mission Global 1 arc second Version 3, , doi:10.5067/MEaSUREs/SRTM/SRTMGL1.003, 2013.

Nuth, C. and Kääb, A.: Co-registration and bias corrections of satellite elevation data sets for quantifying glacier thickness change, The Cryosphere, 5(1), 271–290, doi:10.5194/tc-5-271-2011, 2011.

Paul, F., Barrand, N. E., Baumann, S., Berthier, E., Bolch, T., Casey, K., Frey, H., Joshi, S. P., Konovalov, V., Bris, R. L., Mölg, N., Nosenko, G., Nuth, C., Pope, A., Racoviteanu, A., Rastner, P., Raup, B., Scharrer, K., Steffen, S. and Winsvold, S.: On the accuracy of glacier outlines derived from remote-sensing data, Annals of Glaciology, 54(63), 171–182, doi:10.3189/2013AoG63A296, 2013.

Peduzzi, P., Herold, C. and Silverio, W.: Assessing high altitude glacier thickness, volume and area changes using field, GIS and remote sensing techniques: the case of Nevado Coropuna (Peru), The Cryosphere, 4(3), 313–323, doi:10.5194/tc-4-313-2010, 2010.

Polk, M. H., Young, K. R., Baraer, M., Mark, B. G., McKenzie, J. M., Bury, J. and Carey, M.: Exploring hydrologic connections between tropical mountain wetlands and glacier recession in Peru's Cordillera Blanca, Applied Geography, 78, 94–103, doi:10.1016/j.apgeog.2016.11.004, 2017.

Pouyaud, B., Zapata, M., Yerren, J., Gomez, J., Rosas, G., Suarez, W. and Ribstein, P.: Avenir des ressources en eau glaciaire de la Cordillère Blanche / On the future of the water resources from glacier melting in the Cordillera Blanca, Peru, Hydrological Sciences Journal, 50(6), null-1022, doi:10.1623/hysj.2005.50.6.999, 2005.

Rabatel, A., Bermejo, A., Loarte, E., Soruco, A., Gomez, J., Leonardini, G., Vincent, C. and Sicart, J. E.: Can the snowline be used as an indicator of the equilibrium line and mass balance for glaciers in the outer tropics?, Journal of Glaciology, 58(212), 1027–1036, doi:10.3189/2012JoG12J027, 2012.

Rabatel, A., Francou, B., Soruco, A., Gomez, J., Cáceres, B., Ceballos, J. L., Basantes, R., Vuille, M., Sicart, J.-E., Huggel, C., Scheel, M., Lejeune, Y., Arnaud, Y., Collet, M., Condom, T., Consoli, G., Favier, V., Jomelli, V., Galarraga, R., Ginot, P., Maisincho, L., Mendoza, J., Ménégoz, M., Ramirez, E., Ribstein, P., Suarez, W., Villacis, M. and Wagnon, P.: Current state of glaciers in the tropical Andes: a multi-century perspective on glacier evolution and climate change, The Cryosphere, 7(1), 81–102, doi:10.5194/tc-7-81-2013, 2013.

Racoviteanu, Adina (submitter); Racoviteanu, Adina (analyst(s)), 2005. GLIMS Glacier Database. Boulder, CO. National Snow and Ice Data Center. http://dx.doi.org/10.7265/N5V98602

Racoviteanu, A. E., Manley, W. F., Arnaud, Y. and Williams, M. W.: Evaluating digital elevation models for glaciologic applications: An example from Nevado Coropuna, Peruvian Andes, Global and Planetary Change, 59(1), 110–125, doi:10.1016/j.gloplacha.2006.11.036, 2007.

Racoviteanu, A. E., Arnaud, Y., Williams, M. W. and Ordoñez, J.: Decadal changes in glacier parameters in the Cordillera Blanca, Peru, derived from remote sensing, Journal of Glaciology, 54(186), 499–510, doi:10.3189/002214308785836922, 2008.

Ramirez, E., Francou, B., Ribstein, P., Descloitres, M., Guerin, R., Mendoza, J., Gallaire, R., Pouyaud, B. and Jordan, E.: Small glaciers disappearing in the tropical Andes: a case-study in Bolivia: Glaciar Chacaltaya (16 o S), Journal of Glaciology, 47(157), 187–194, 2001.

RGI Consortium: Randolph Glacier Inventory – A Dataset of Global Glacier Outlines: Version 6.0: Technical Report, Global Land Ice Measurements from Space, , doi:10.7265/N5-RGI-60, 2017.

Rolstad, C., Haug, T. and Denby, B.: Spatially integrated geodetic glacier mass balance and its uncertainty based on geostatistical analysis: application to the western Svartisen ice cap, Norway, Journal of Glaciology, 55(192), 666–680, doi:10.3189/002214309789470950, 2009.

Rossi, C., Minet, C., Fritz, T., Eineder, M. and Bamler, R.: Temporal monitoring of subglacial volcanoes with TanDEM-X — Application to the 2014–2015 eruption within the Bárðarbunga volcanic system, Iceland, Remote Sensing of Environment, 181, 186–197, doi:10.1016/j.rse.2016.04.003, 2016.

Sagredo, E. A. and Lowell, T. V.: Climatology of Andean glaciers: A framework to understand glacier response to climate change, Global and Planetary Change, (86–87), 101–109, 2012.

Salzmann, N., Huggel, C., Rohrer, M., Silverio, W., Mark, B. G., Burns, P. and Portocarrero, C.: Glacier changes and climate trends derived from multiple sources in the data scarce Cordillera Vilcanota region, southern Peruvian Andes, The Cryosphere, 7(1), 103–118, doi:10.5194/tc-7-103-2013, 2013.

Schauwecker, S., Rohrer, M., Huggel, C., Endries, J., Montoya, N., Neukom, R., Perry, B., Salzmann, N., Schwarb, M. and Suarez, W.: The freezing level in the tropical Andes, Peru: An indicator for present and future glacier extents, J. Geophys. Res. Atmos., 122(10), 2016JD025943, doi:10.1002/2016JD025943, 2017.

Seehaus, T., Marinsek, S., Helm, V., Skvarca, P. and Braun, M.: Changes in ice dynamics, elevation and mass discharge of Dinsmoor–Bombardier–Edgeworth glacier system, Antarctic Peninsula, Earth and Planetary Science Letters, 427, 125–135, doi:10.1016/j.epsl.2015.06.047, 2015.

Silverio, W. and Jaquet, J.-M.: Glacial cover mapping (1987–1996) of the Cordillera Blanca (Peru) using satellite imagery, Remote Sensing of Environment, 95(3), 342–350, doi:10.1016/j.rse.2004.12.012, 2005.

Silverio, W. and Jaquet, J.-M.: Multi-temporal and multi-source cartography of the glacial cover of Nevado Coropuna (Arequipa, Peru) between 1955 and 2003, International Journal of Remote Sensing, 33(18), 5876–5888, doi:10.1080/01431161.2012.676742, 2012.

Silverio, W. and Jaquet, J.-M.: Evaluating glacier fluctuations in Cordillera Blanca (Peru), Archives des SCIENCES, 18, 2017.

Soruco, A., Vincent, C., Francou, B. and Gonzalez, J. F.: Glacier decline between 1963 and 2006 in the Cordillera Real, Bolivia, Geophys. Res. Lett., 36(3), L03502, doi:10.1029/2008GL036238, 2009a.

Soruco, A., Vincent, C., Francou, B., Ribstein, P., Berger, T., Sicart, J. E., Wagnon, P., Arnaud, Y., Favier, V. and Lejeune, Y.: Mass balance of Glaciar Zongo, Bolivia, between 1956 and 2006, using glaciological, hydrological and geodetic methods, Annals of Glaciology, 50(50), 1–8, doi:10.3189/172756409787769799, 2009b.

Toutin, T.: Three-dimensional topographic mapping with ASTER stereo data in rugged topography, IEEE Transactions on Geoscience and Remote Sensing, 40(10), 2241–2247, doi:10.1109/TGRS.2002.802878, 2002.

Ubeda, J.: El impacto del cambio climático en los glaciares del complejo volcánico Nevado Coropuna, (Cordillera Occidental de los Andes Centrales), info:eu-repo/semantics/doctoralThesis, Universidad Complutense de Madrid, Servicio de Publicaciones, Madrid, 13 April. [online] Available from: https://eprints.ucm.es/12076/ (Accessed 26 October 2018), 2011.

UGRH: INVENTARIO DE GLACIARES CORDILLERA BLANCA, , 81, 2010.

UGRH: Inventario de glaciares del Peru, 2014.

Ulaby, F. T., Stiles, W. H. and Abdelrazik, M.: Snowcover Influence on Backscattering from Terrain, IEEE Transactions on Geoscience and Remote Sensing, GE-22(2), 126–133, doi:10.1109/TGRS.1984.350604, 1984.

Veettil, B. K.: Glacier mapping in the Cordillera Blanca, Peru, tropical Andes, using Sentinel-2 and Landsat data, Singapore Journal of Tropical Geography, 39(3), 351–363, doi:10.1111/sjtg.12247, 2018.

Veettil, B. K. and Kamp, U.: Remote sensing of glaciers in the tropical Andes: a review, International Journal of Remote Sensing, 38(23), 7101–7137, doi:10.1080/01431161.2017.1371868, 2017.

Veettil, B. K. and Souza, S. F. de: Study of 40-year glacier retreat in the northern region of the Cordillera Vilcanota, Peru, using satellite images: preliminary results, Remote Sensing Letters, 8(1), 78–85, doi:10.1080/2150704X.2016.1235811, 2017.

Veettil, B. K., Bremer, U. F., Souza, S. F. de, Maier, É. L. B. and Simões, J. C.: Variations in annual snowline and area of an ice-covered stratovolcano in the Cordillera Ampato, Peru, using remote sensing data (1986–2014), Geocarto International, 31(5), 544–556, doi:10.1080/10106049.2015.1059902, 2016.

Veettil, B. K., Souza, S. F. de, Simões, J. C. and Pereira, S. F. R.: Decadal evolution of glaciers and glacial lakes in the Apolobamba–Carabaya region, tropical Andes (Bolivia–Peru), Geografiska Annaler: Series A, Physical Geography, 99(3), 193–206, doi:10.1080/04353676.2017.1299577, 2017a.

Veettil, B. K., Wang, S., Florêncio de Souza, S., Bremer, U. F. and Simões, J. C.: Glacier monitoring and glacier-climate interactions in the tropical Andes: A review, Journal of South American Earth Sciences, 77, 218–246, doi:10.1016/j.jsames.2017.04.009, 2017b.

Veettil, B. K., Wang, S., Bremer, U. F., de Souza, S. F. and Simões, J. C.: Recent trends in annual snowline variations in the northern wet outer tropics: case studies from southern Cordillera Blanca, Peru, Theoretical Applied Climatology, 129(1), 213–227, doi:10.1007/s00704-016-1775-0, 2017c.

Veettil, B. K., Wang, S., Simões, J. C., Ruiz Pereira, S. F. and de Souza, S. F.: Regional climate forcing and topographic influence on glacier shrinkage: eastern cordilleras of Peru, International Journal of Climatology, 38(2), 979–995, doi:10.1002/joc.5226, 2017d.

Vijay, S. and Braun, M.: Elevation Change Rates of Glaciers in the Lahaul-Spiti (Western Himalaya, India) during 2000–2012 and 2012–2013, Remote Sensing, 8(12), 1038, doi:10.3390/rs8121038, 2016.

Vuille, M.: Climate Change and Water Resources in the Tropical Andes, Inter-American Development Bank, 2013.

Vuille, M., Kaser, G. and Juen, I.: Glacier mass balance variability in the Cordillera Blanca, Peru and its relationship with climate and the large-scale circulation, Global and Planetary Change, 62(1), 14–28, doi:10.1016/j.gloplacha.2007.11.003, 2008.

Vuille, M., Carey, M., Huggel, C., Buytaert, W., Rabatel, A., Jacobsen, D., Soruco, A., Villacis, M., Yarleque, C., Elison Timm, O., Condom, T., Salzmann, N. and Sicart, J.-E.: Rapid decline of snow and ice in the tropical Andes – Impacts, uncertainties and challenges ahead, Earth-Science Reviews, 176(Supplement C), 195–213, doi:10.1016/j.earscirev.2017.09.019, 2018.

Wagnon, P., Ribstein, P., Francou, B. and Pouyaud, B.: Annual cycle of energy balance of Zongo Glacier, Cordillera Real, Bolivia, J. Geophys. Res., 104(D4), 3907–3923, doi:10.1029/1998JD200011, 1999.

Wagnon, P., Ribstein, P., Francou, B. and Sicart, J. E.: Anomalous heat and mass budget of Glaciar Zongo, Bolivia, during the 1997/98 El Niño year, Journal of Glaciology, 47(156), 21–28, doi:10.3189/172756501781832593, 2001.

WGMS: Fluctuations of Glaciers 1990-1995., n.d.

Zink, M., Bartusch, M. and Miller, D.: TanDEM-X Mission Status, in IEEE International Geoscience and Remote Sensing Symposium (IGARSS), pp. 1–4. [online] Available from: http://elib.dlr.de/70355/, 2011.
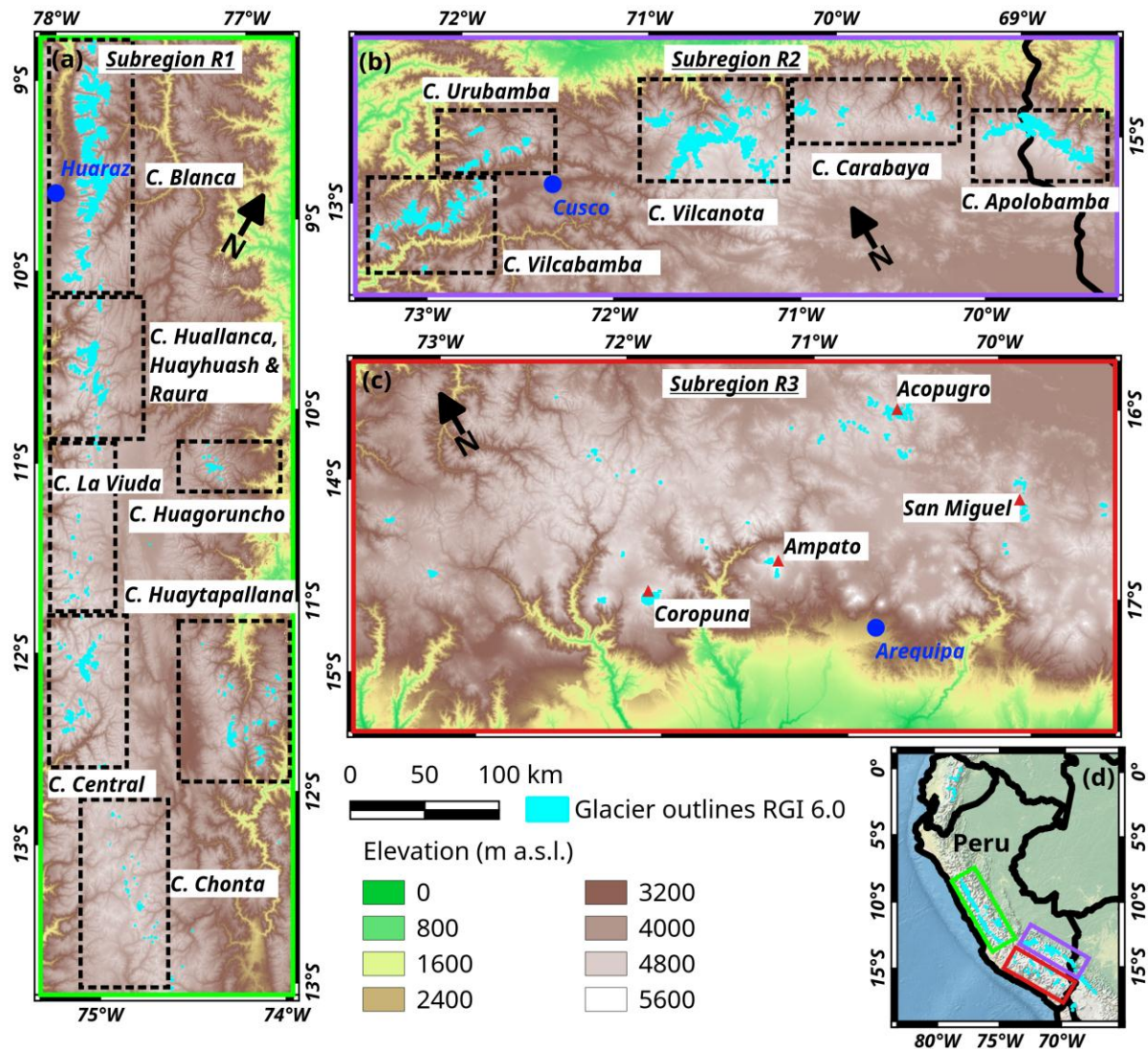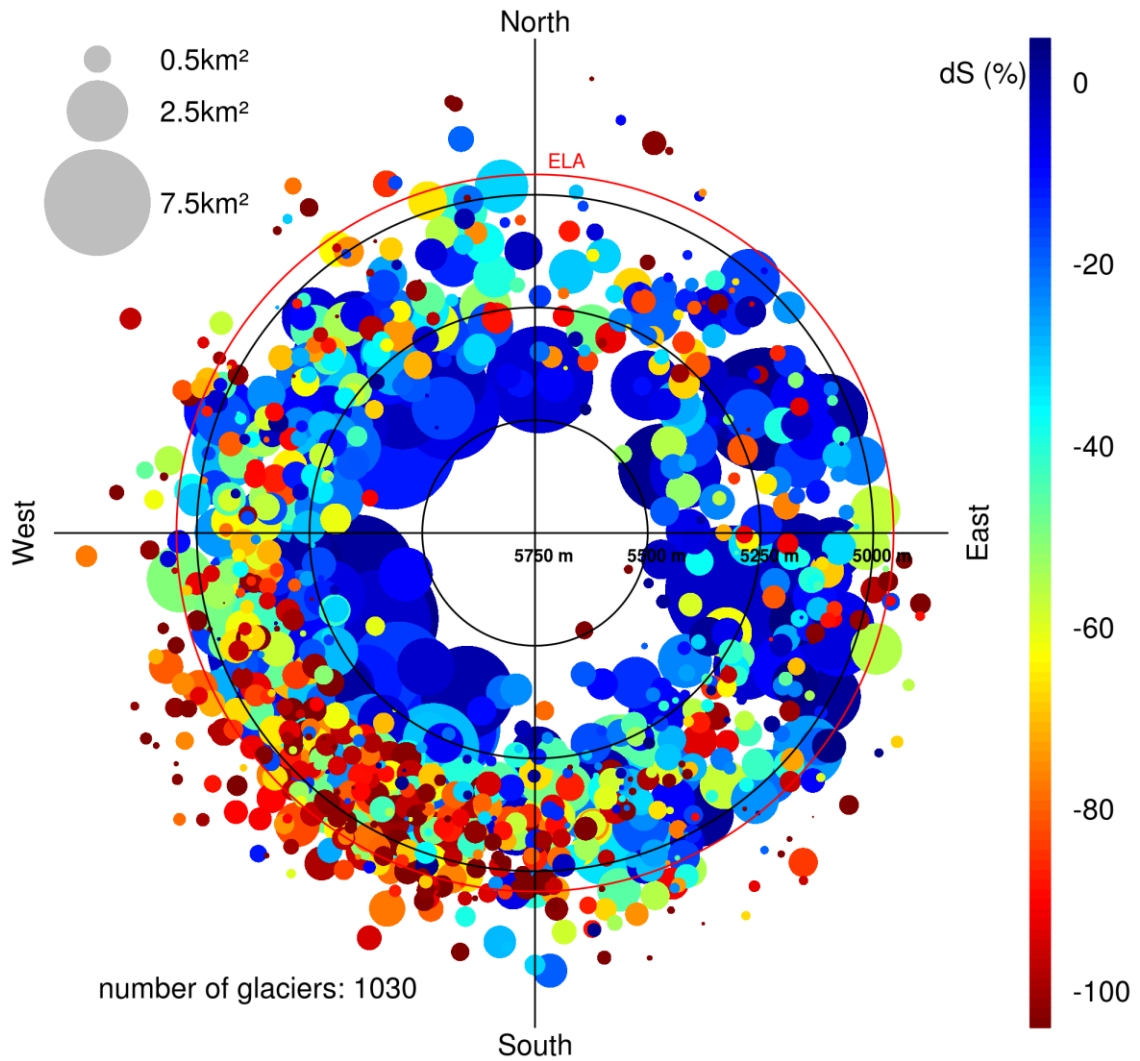
Figures:

Figure 1. General maps of study region. Panels (a-c): glacier subregions in Peru according to Sagredo and Lowell (2012); (a) subregion R1: northern wet outer tropics; (b) subregion R2: southern wet outer tropics; (c) subregion R3: dry outer tropics. Panel (d): overview map of Peru. Coloured rectangles indicate the locations of the subregions (same frame colours). Light blue areas: glacier coverage based on RGI 6.0. Background: SRTM DEM © NASA
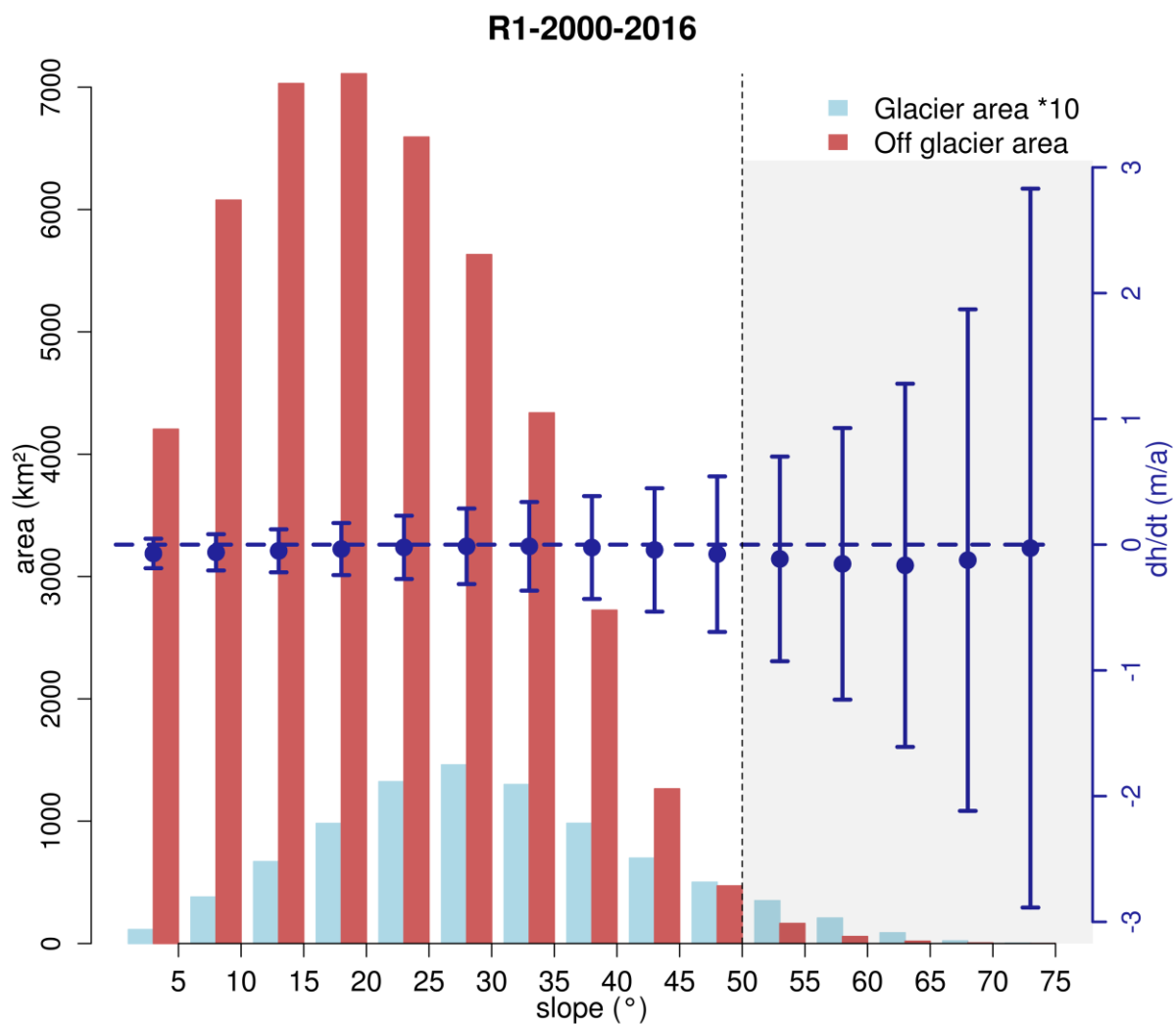
Figure 2. Off-(red) and on-glacier (light blue) area and off-glacier elevation change (blue dots) distributions in dependency on slope in subregion R1 for the period 2000-2016. Error bars represent NMAD of Δh/Δt values in the individual slope interval. Dotted line indicates the applied slope threshold (see Section 4.2). Glacier area measurements are based on the glacier outlines from 2000. Note: For better representation, on-glacier areas are scaled by a factor of 10. Plots for other subregions are provided in the Supplementary material.

Figure 3. Polar plot of relative area changes (dot colour) in subregion R1 in the period 2000-2016 of individual glaciers. Dot size: glacier size in 2000; Radius: median elevation; Orientation: mean aspect. Red circle: equilibrium line altitude (ELA), see also Table S3. Plots for other subregions and time intervals are provided in the Supplementary material.
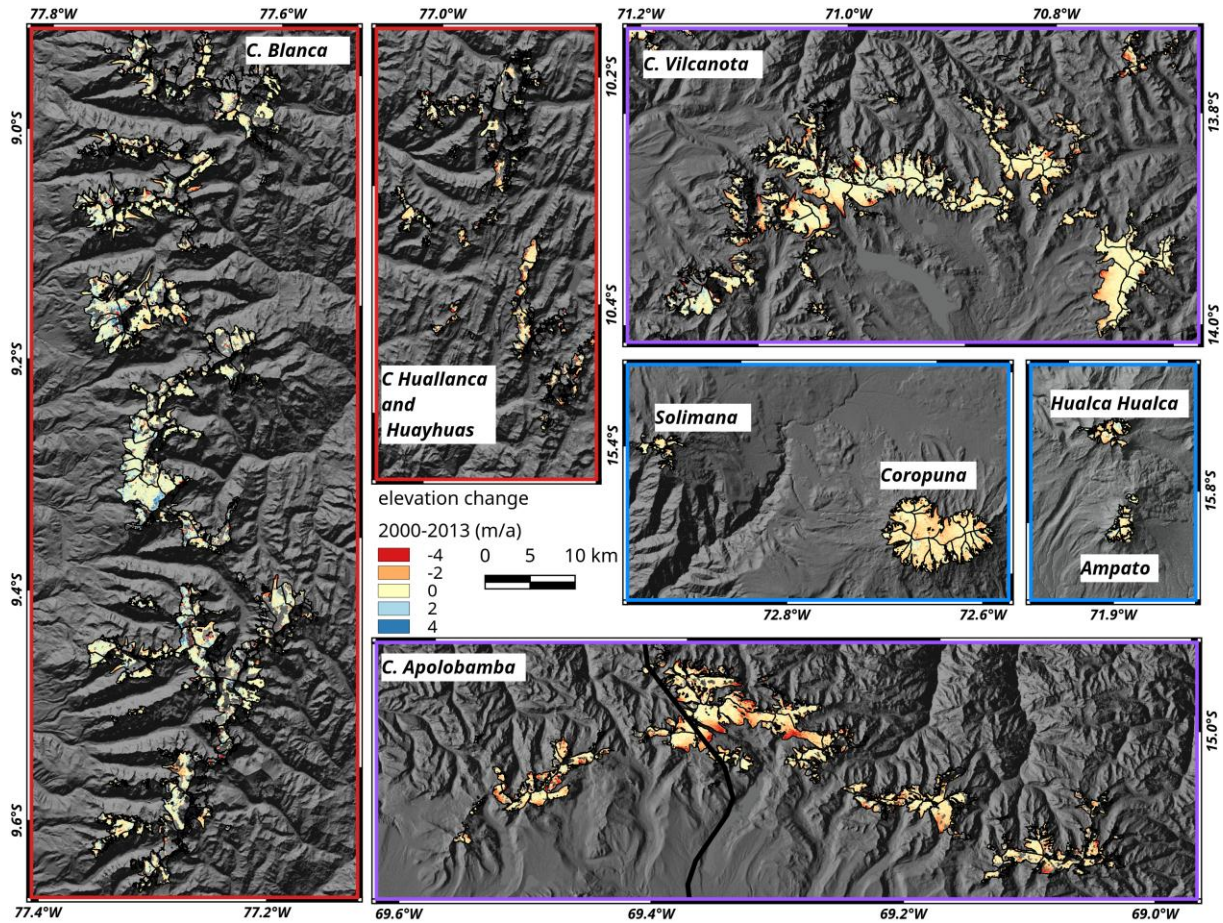
Figure 4. Surface elevation changes in the period 2000-2013 at mountain ranges in all three subregions (unfiltered). The frame colour of the panels indicates the subregions (see **Figure 1**). Background: SRTM DEM hillshade © NASA
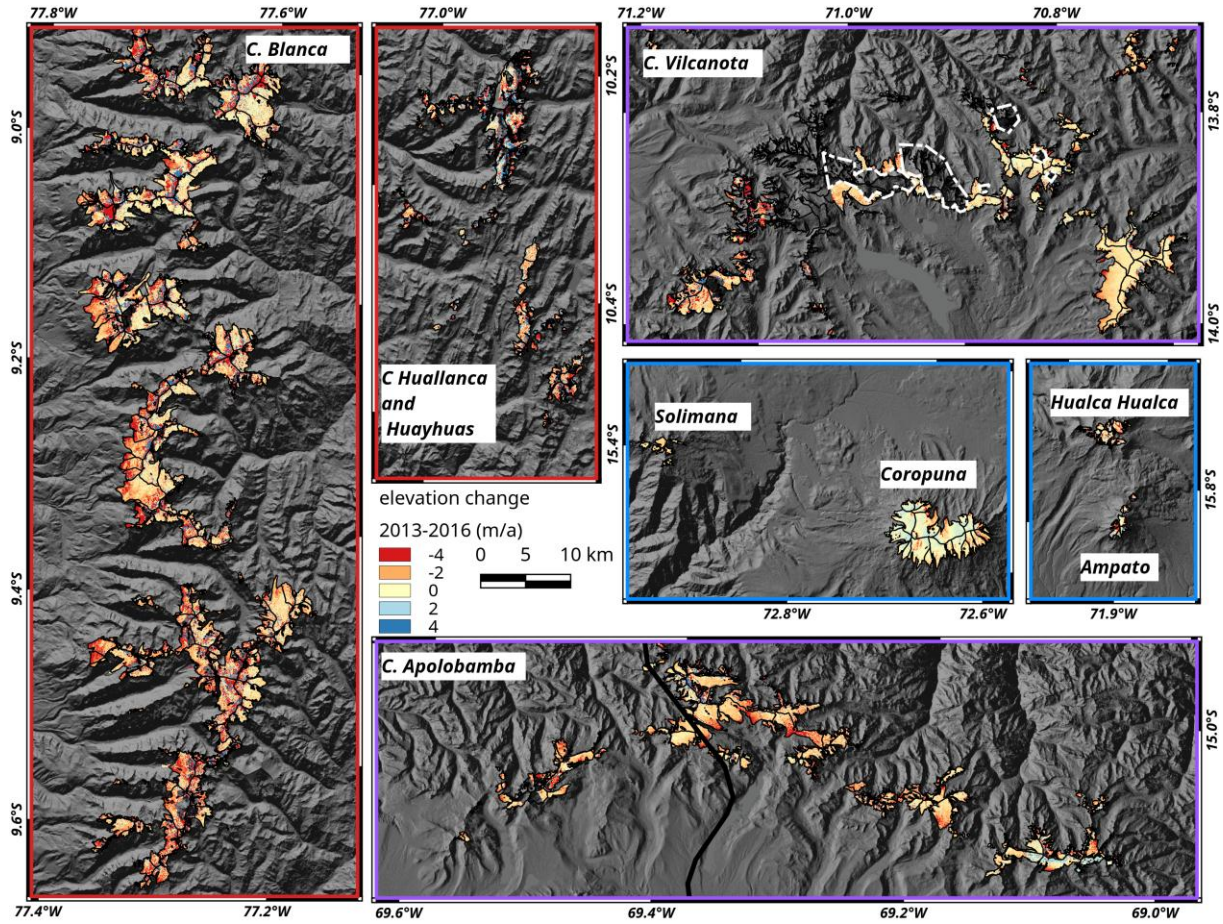
Figure 5. Surface elevation changes in the period 2013-2016 at mountain ranges in all three subregions (unfiltered). The frame colour of the panels indicates the subregions (see **Figure 1**). White dashed line: masked out areas affected by phase jumps in the unwrapped interferogram. Background: SRTM DEM hillshade © NASA
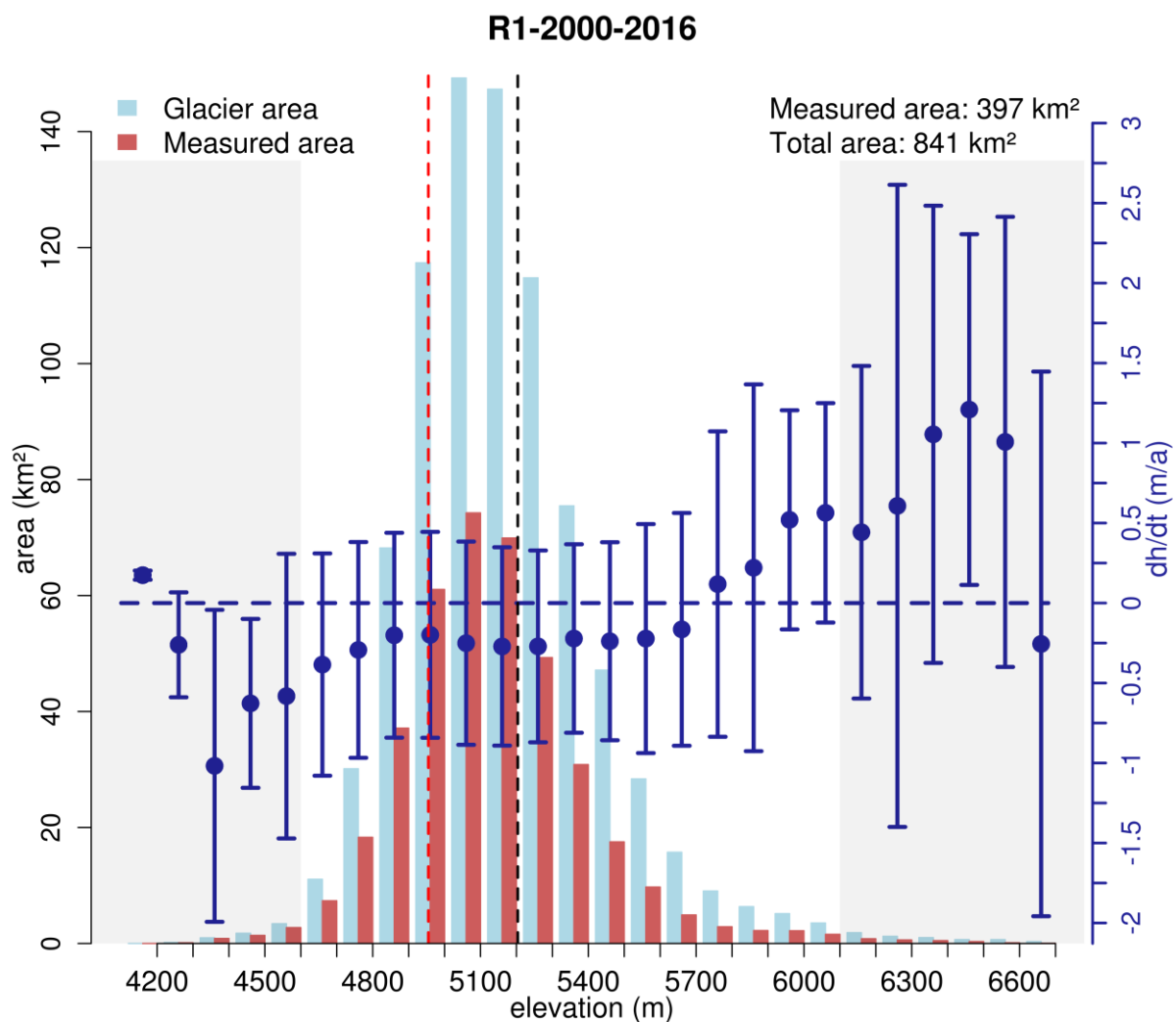
Figure 6. Hypsometric distribution of measured (red bars) and total (light blue bars) glacier area with elevation in subregion R1 in the interval 2000-2016. Blue dots represent the mean Δh/Δt value in each elevation interval. Error bars indicate NMAD of Δh/Δt for each hypsometric bin. Grey areas mark the lower and upper 1% quantile of the total glacier area distribution. Black dashed line: mean glacier elevation; Red dashed line: equilibrium line altitude (ELA), see also Table S3. Area measurements are based on the glacier outlines from 2000, considering only regions with slopes below applied slope threshold (50°, see Section 4.2). Plots for other subregions are provided in the Supplementary material.
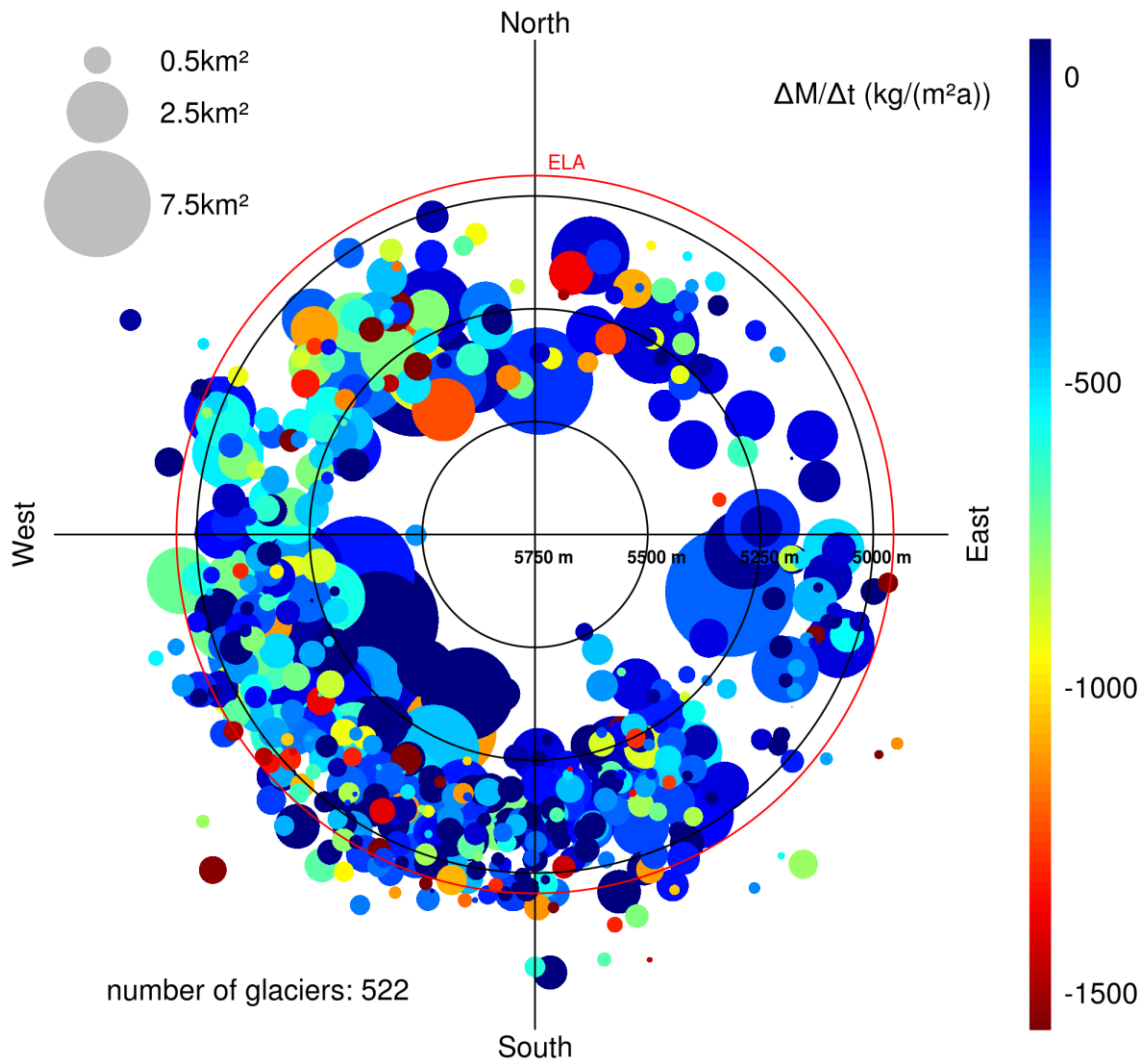
Figure 7. Polar plot of specific mass balance (dot colour) of individual glaciers in subregion R1 in the period 2000-2016 of individual glaciers. Dot size: glacier size in 2000; Radius: median elevation; Orientation: mean aspect. Red circle: equilibrium line altitude (ELA), see also Table S3. Note: only glaciers with elevation change information >50% are included. Plots for other subregions and time intervals are provided in the Supplementary material.
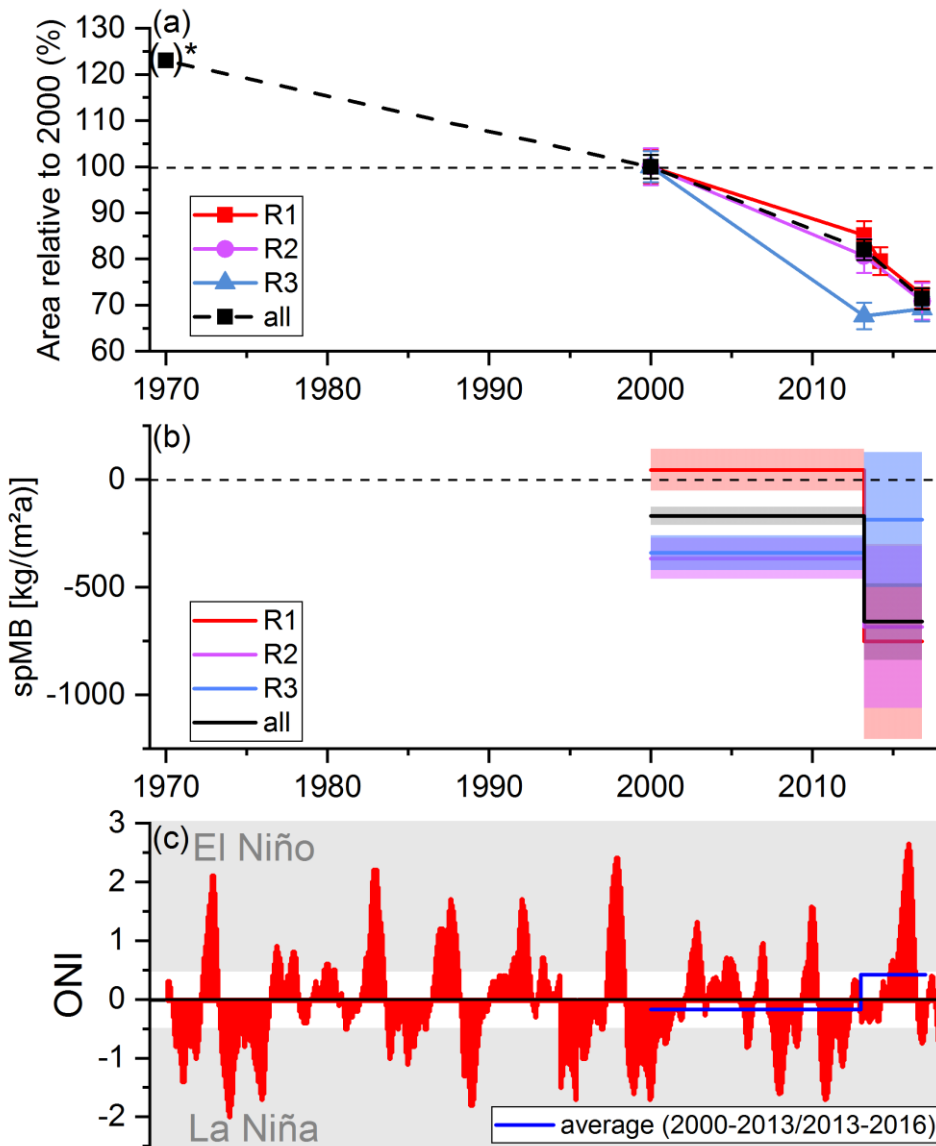
Figure 8. Temporal evolution of (a) relative glacier area changes, (b) observed specific mass balance (spMB, colour shaded areas represent the uncertainty of the corresponding measurements) and (c) Oceanic Nino Index (ONI) in the period 1970-2016. *Area measurement in 1970 taken from the 1st Peruvian Glacier Inventory (Hidrandina SA, 1986) and only mountain ranges with complete coverage by the inventory in 1970 are considered in the area change computation (see also Section 6.1)

Tables:

Table 1. Measured glacier extents for different years and regions.

year	S (km²)	δ_S (km²)	n
Subregion R1			
2000	910.1	32.3	1162
2013	774.9	27.6	1159
2016	657.0	26.7	1088
Subregion R2			
2000	893.9	35.7	702
2013	720.8	33.0	639
2016	633.2	35.5	633
Subregion R3			
2000	112.6	3.8	109
2013	76.2	3.2	104
2016	77.9	3.0	82
All subregions (country wide)			
2000	1916.6	48.3	1973
2013	1571.9	43.1	1903
2016	1368.1	44.5	1803

_____

S: measured glacier area
δ_S: uncertainty of measured glacier area
n: number of glacier catchments (delineations based on RGI 6.0)

Table 2. Measured area, surface and mass changes for different periods and regions. [+]constant volume to mass conversion factor of 850 kg m⁻³; [o] volume to mass conversion factor of 600 kg m⁻³ and 900 kg m⁻³ for region below and above the ELA (Table S3), respectively; *mean glacier area of observation interval is used to calculate specific mass balances (see Section 4.3)

period	dt a	dS km²	%	dS/dt Km² a⁻¹	dh_M/dt m a⁻¹	dh_E/dt m a⁻¹	S_M %	$\Delta M/\Delta t$ [+] Gt a⁻¹	kg m⁻² a⁻¹*	ΔM [+] Gt	$\Delta M/\Delta t$ [o] Gt a⁻¹	kg m⁻² a⁻¹*	ΔM [o] Gt
Subregion R1													
2000-2012	11.98	-	-	-	-0.024±0.067	-0.017±0.104	46	-0.012±0.087	-15±111	-0.15±1.04	-0.011±0.083	-15±105	-0.14±0.99
2000-2013	12.94	-135.2±42.5	-15	-10.4	0.055±0.61	0.073±0.093	48	0.053±0.008	68±102	0.68+1.03	0.036±0.008	45±97	0.46±0.98
2000-2016	16.65	-253.2±41.9	-27	-15.8	-0.236±0.042	-0.208±0.065	47	-0.148±0.077	-205±107	-2.47±1.28	-0.113±0.073	-157±102	-1.89±1.22
2013-2016	3.71	-117.9±38.4	-15	-39.3	-1.208±0.228	-1.067±0.273	80	-0.649±0.312	-990±476	-2.41±1.16	-0.493±0.296	-752±452	-1.83±1.10
Subregion R2													
2000-2013	13.02	-173.1±48.6	-20	-12.4	-0.400±0.069	-0.440±0.095	61	-0.318±0.077	-412±100	-4.14±1.01	-0.283±0.073	-366±95	-3.68±0.96
2000-2016	16.68	-260.6±50.4	-29	-16.3	-0.500±0.050	-0.512±0.074	53	-0.371±0.064	-511±88	-6.19±1.06	-0.316±0.061	-435±84	-5.28±1.01
2013-2016	3.67	-87.6±48.5	-12	-43.8	-0.972±0.187	-0.916±0.244	69	-0.538±0.256	-834±396	-1.97±0.94	-0.442±0.243	-685±376	-1.62±0.89
Subregion R3													
2000-2013	12.93	-36.4±5.0	-32	-2.6	-0.390±0.047	-0.394±0.052	89	-0.038±0.008	-395±85	-0.49±0.11	-0.032±0.008	-340±81	-0.41±0.10
2000-2016	16.65	-34.7±4.9	-31	-2.2	-0.322±0.037	-0.328±0.042	87	-0.031±0.007	-328±74	-0.52±0.11	-0.027±0.007	-288±70	-0.45±0.10
2013-2016	3.71	1.7±4.4	2	0.9	-0.231±0.187	-0.210±0.208	89	-0.014±0.025	-184±329	-0.05±0.09	-0.014±0.024	-186±313	-0.05±0.09
All subregions (country wide)													
2000-2013	12.98	-344.7±64.8	-18	-24.6	-0.220±0.064	-0.198±0.091	56.9	-0.302±0.074	-184±45	-4.43±1.00	-0.279±0.070	-169±43	-3.64±0.95
2000-2016	16.66	-548.5±65.7	-29	-34.3	-0.370±0.045	-0.359±0.068	52.2	-0.550±0.067	-357±43	-9.18±1.10	-0.457±0.064	-296±41	-7.62±1.05
2013-2016	3.69	-203.8±62.0	-13	-101.9	-1.049±0.208	-0.953±0.256	75.6	-1.201±0.271	-836±188	-3.95±0.96	-0.949±0.257	-660±178	-3.50±0.91

_____

dt: observation period (mean time lag between DEM dates)
dS: glacier area change
dS/dt: glacier area change rate (mean time lag between glacier inventories is used)
dh_M/dt: average measured surface lowering rate
dh_E/dt: average extrapolated surface lowering rate
S_M: fraction of glacier area covered by dh_M/dt measurements (below slope threshold)
$\Delta M/\Delta t$: mass balance (average and specific)
ΔM: Total mass change in the observation period